Positive feedback between NF-κB and TNF-α promotes leukemia-initiating cell capacity

Yuki Kagoya,[1] Akihide Yoshimi,[1] Keisuke Kataoka,[1] Masahiro Nakagawa,[1] Keiki Kumano,[1] Shunya Arai,[1] Hiroshi Kobayashi,[2] Taku Saito,[2] Yoichiro Iwakura,[3] and Mineo Kurokawa[1]

[1]Department of Hematology and Oncology and [2]Department of Orthopaedic Surgery, Graduate School of Medicine, The University of Tokyo, Tokyo, Japan. [3]Division of Experimental Animal Immunology, Research Institute for Biomedical Sciences, Tokyo University of Science, Chiba, Japan.

Acute myeloid leukemia (AML) is a heterogeneous hematologic malignancy that originates from leukemia-initiating cells (LICs). The identification of common mechanisms underlying LIC development will be important in establishing broadly effective therapeutics for AML. Constitutive NF-κB pathway activation has been reported in different types of AML; however, the mechanism of NF-κB activation and its importance in leukemia progression are poorly understood. Here, we analyzed myeloid leukemia mouse models to assess NF-κB activity in AML LICs. We found that LICs, but not normal hematopoietic stem cells or non-LIC fractions within leukemia cells, exhibited constitutive NF-κB activity. This activity was maintained through autocrine TNF-α secretion, which formed an NF-κB/TNF-α positive feedback loop. LICs had increased levels of active proteasome machinery, which promoted the degradation of IκBα and further supported NF-κB activity. Pharmacological inhibition of the proteasome complex markedly suppressed leukemia progression in vivo. Conversely, enhanced activation of NF-κB signaling expanded LIC frequency within leukemia cell populations. We also demonstrated a strong correlation between NF-κB activity and TNF-α secretion in human AML samples. Our findings indicate that NF-κB/TNF-α signaling in LICs contributes to leukemia progression and provide a widely applicable approach for targeting LICs.

Introduction

Acute myeloid leukemia (AML) is a highly aggressive hematologic malignancy characterized by a relentless proliferation of immature myeloid blasts. Recent studies have demonstrated that the apparently uniform leukemia cell population is organized as a hierarchy that originates from leukemia-initiating cells (LICs) (1, 2). Although intensive chemotherapy is initially effective in most cases of AML, the surviving LIC clones repopulate the disease, leading to subsequent relapse and an ultimately dismal prognosis (3). Another problem is that AML is a heterogeneous disease with different cytogenetic and molecular abnormalities. This heterogeneity has increasingly been unveiled by recent work involving the screening of recurrent mutations seen in AML cells using high-throughput sequencing technology, which is useful for constructing individualized therapeutics (4, 5). At the same time, however, these findings indicate that it is difficult to develop a treatment strategy in addition to standard chemotherapy that is widely applicable to AML. Therefore, to establish effective treatments, it is important to identify the universally essential mechanisms involved in the LIC phenotype, irrespective of the cells' diverse genetic abnormalities.

NF-κB is a transcription factor initially discovered in B cells (6). Although well known for its role in controlling various aspects of immune responses, the NF-κB pathway is now also recognized as an important regulator of cell survival, proliferation, and differentiation (7–9). Its constitutive activation has been reported in a variety of malignancies and mostly plays a cancer-promoting role (10–12). There is some evidence that this pathway activity is also seen in the AML $CD34^+CD38^-$ fraction, which is considered to be enriched for LICs (13, 14). Given that NF-κB activity is not restricted to specific AML subtypes or genetic abnormalities, it is possible that the signaling is universally essential for myeloid leukemia progression, and a variety of agents have been reported to induce apoptosis in cultured leukemia cells via NF-κB pathway inhibition (15–19). The effect of specific inhibition of the NF-κB pathway on LICs in vivo, however, has not been sufficiently studied. Furthermore, the mechanism of this pathway's activation remains to be elucidated. Although several gene mutations found in hematologic malignancies have been reported to be associated with enhanced NF-κB signaling (20–22), these findings do not fully explain why the activation of NF-κB is observed in a number of different types of leukemia. It is more intriguing, as well as reasonable, to consider that NF-κB activation arises from the signaling pathways that are commonly involved in LICs. Another limitation of the previous studies is that LIC-enriched populations in AML are highly heterogeneous among patients and are not necessarily confined to the $CD34^+CD38^-$ fraction, as they are in normal HSCs. Therefore, it is problematic to strictly define LICs by their surface-marker antigens (23, 24).

To overcome these challenges, we used variable myeloid leukemia mouse models, in which LIC-enriched fractions were well characterized using a surface marker phenotype and revealed that NF-κB signaling is constitutively activated in LICs, but not in normal cells or non-LIC fractions within leukemic BM cells. We also elucidate the mechanism of NF-κB activation in LICs in each model and demonstrate that the inhibition of NF-κB or its upstream machinery in LICs markedly suppresses leukemia progression in vivo.

Results

The NF-κB pathway is activated in LICs of different types of myeloid leukemia models. To extensively investigate NF-κB activity in LICs of

Conflict of interest: The authors have declared that no conflict of interest exists.
Citation for this article: *J Clin Invest.* doi:10.1172/JCI68101.

different types of myeloid leukemia, we used three types of mouse models of myeloid leukemia induced by the retroviral transduction of granulocyte-monocyte progenitors (GMPs) with MLL-ENL and MOZ-TIF2 and the cotransduction of GMPs with BCR-ABL and NUP98-HOXA9 (Supplemental Figure 1; supplemental material available online with this article; doi:10.1172/JCI68101DS1). LIC-enriched populations of these myeloid leukemia models have been investigated in previous studies: GMP-like leukemia cells (L-GMPs) in MLL-ENL and MOZ-TIF2 models and the lineage$^-$ Sca-1$^+$ fraction in the BCR-ABL/NUP98-HOXA9 model (Supplemental Figure 2, A–C, and refs. 25–27). In order to obtain cell populations that would barely contain LICs, we also sorted lineage$^-$ c-Kit$^-$ cells in MLL-ENL and MOZ-TIF2 leukemic mice and lineage$^+$ cells in a BCR-ABL/NUP98-HOXA9 model. There were striking differences in clonogenic potential (Supplemental Figure 3) and LIC frequencies, as determined by in vivo limiting dilution assays in the two populations of each model (Figure 1A and Supplemental Table 1). Therefore, we confirmed that LIC and non-LIC fractions can be clearly isolated through the surface antigen profiles of the three leukemia models. Next, we visualized the subcellular distribution of the major NF-κB subunit p65 in LICs, non-LICs, and normal cells by immunofluorescence staining and confocal microscopy. As shown in Figure 1B, prominent nuclear translocation of p65 was observed in the LICs of each model, while it was retained mostly in the cytoplasm in normal lineage$^-$ c-Kit$^+$ Sca-1$^+$ cells (KSLs), which are enriched for HSCs and GMPs. Interestingly, non-LICs also had relatively reduced p65 nuclear translocation signal compared with that in LICs in all three leukemia models. We quantified the nucleus/cytoplasm ratio of p65 staining intensity in these images, which also showed that the LICs in each model had significant nuclear localization compared with that observed in non-LICs, normal KSLs, and GMPs (Figure 1C).

To further test NF-κB transcription activity in LICs, we investigated the expression profiles of a subset of genes regulated by the NF-κB pathway. We first used two sets of published gene expression microarray data, which compared the expression profiles of MOZ-TIF2 L-GMPs (26), MLL-AF9 L-GMPs, and HOXA9-MEIS1 L-GMPs (28) with those of normal hematopoietic stem or progenitor cells (HSPCs). The expression profiles of previously identified NF-κB target genes were assessed by gene set enrichment analysis (GSEA) (Supplemental Table 2 and ref. 29), which showed that L-GMPs had increased expression levels of NF-κB target genes compared with those in normal HSPCs in both sets of gene expression microarray data (Figure 2A). We also compared the expression profiles of the same gene set in CD34$^+$CD38$^-$ human AML cells with those of the equivalent cell population in normal BM cells, which corresponded to the HSC fraction, and observed a similar tendency (Figure 2B and ref. 30). Then, we validated these results using quantitative real-time PCR by comparing the expression levels of several NF-κB target genes in LICs and non-LICs from our three mouse models with those in normal GMPs and found increased expression levels of most of the genes in different types of LICs, but no significant elevation of these levels in non-LICs (Figure 2C and Supplemental Figure 4). Furthermore, the level of p65 phosphorylation, which is important for enhancing its transcription activity, was significantly increased in LICs compared with the level observed in normal GMPs (Figure 2D). Consistent with these findings, LICs showed a more prominent increase in apoptosis than did normal cells or non-LICs when treated with sc-514, a selective inhibitor of IκB kinase β (IKKβ) (Figure 2, E and F, and ref. 31). Although LICs from BCR-ABL/NUP98-HOXA9–induced leukemia were rather resistant to sc-514 compared with cells from MLL-ENL– and MOZ-TIF2–induced leukemia, they still showed higher sensitivity than non-LICs. Collectively, these data fully support the hypothesis that the NF-κB pathway is constitutively activated in the LICs of different types of myeloid leukemia.

LICs maintain their constitutive NF-κB activity via autocrine TNF-α signaling. In the next step, we addressed the question of how LICs maintain constitutive NF-κB activity in different types of leukemia models. In order to investigate genes prevalently dysregulated in LICs, we analyzed the previously published microarray-based gene expression profiles comparing murine and human LICs with normal HSPCs (26, 28, 30). After narrowing down our analysis to the genes commonly upregulated in LICs in three different types of murine leukemia models, we further selected nineteen genes whose expression is elevated in human AML CD34$^+$CD38$^-$ cells (Figure 3A). Among the nineteen genes with typically elevated expression levels in LICs, we focused on *Tnf*, because it is well known as an activator of NF-κB and as an NF-κB–regulated gene. For the purpose of directly evaluating TNF-α abundance in the BM of leukemic mice, we measured the concentration of TNF-α in the BM extracellular fluid and confirmed that it was conspicuously enriched in leukemic BM cells compared with normal BM cells (Figure 3B). We also examined the TNF-α concentration in culture media conditioned by LICs, non-LICs, and normal cells, respectively, to determine whether leukemia cells themselves have the ability to secrete TNF-α. We found that TNF-α secretion was distinctly elevated in LICs, while the normal GMP-conditioned media barely included TNF-α (Figure 3C). Although non-LICs also had TNF-α secretory ability, it was much lower that that of LICs. We therefore reasoned that LICs might maintain their NF-κB pathway activity via autocrine TNF-α signaling. To test this hypothesis, we cultured freshly isolated LICs in serum-free media with a TNF-α–neutralizing antibody or its isotype control and observed p65 subcellular distribution. While LICs treated with isotype control antibodies maintained p65 nuclear translocation even after serum-deprived culture, the p65 translocation signal we observed in three types of LICs was significantly attenuated when these cells were cultured with neutralizing antibodies against TNF-α (Figure 3D). The results were also confirmed by quantification of p65 intensity (Figure 3E). These data strongly suggest that different types of LICs have a similarly increased potential for TNF-α secretion, which maintains constitutive NF-κB activity in an autonomous fashion.

Autocrine TNF-α signaling promotes leukemia cell progression. We were then interested in exploring the effect of autocrine TNF-α secretion on leukemia progression. BM cells derived from WT or *Tnf*-knockout mice were transplanted into sublethally irradiated WT recipient mice after transduction with MLL-ENL and MOZ-TIF2, and cotransduction with BCR-ABL and NUP98-HOXA9 (Figure 3F). Although several mice did develop leukemia with prolonged latency, *Tnf*-deficient cells were significantly ($P < 0.01$) impaired in their ability to initiate leukemia (Figure 3G). We confirmed that *Tnf*-deficient LICs show a distinct decrease in nuclear localization of p65 compared with the that in LICs derived from WT BM cells (Supplemental Figure 5, A and B). Next, we examined whether paracrine TNF-α from the BM microenvironment contributes to leukemia progression. When the established leukemia cells were secondarily transplanted into WT or *Tnf*-knockout recipient mice, *Tnf*-deficient leukemia cells failed to effectively establish AML in

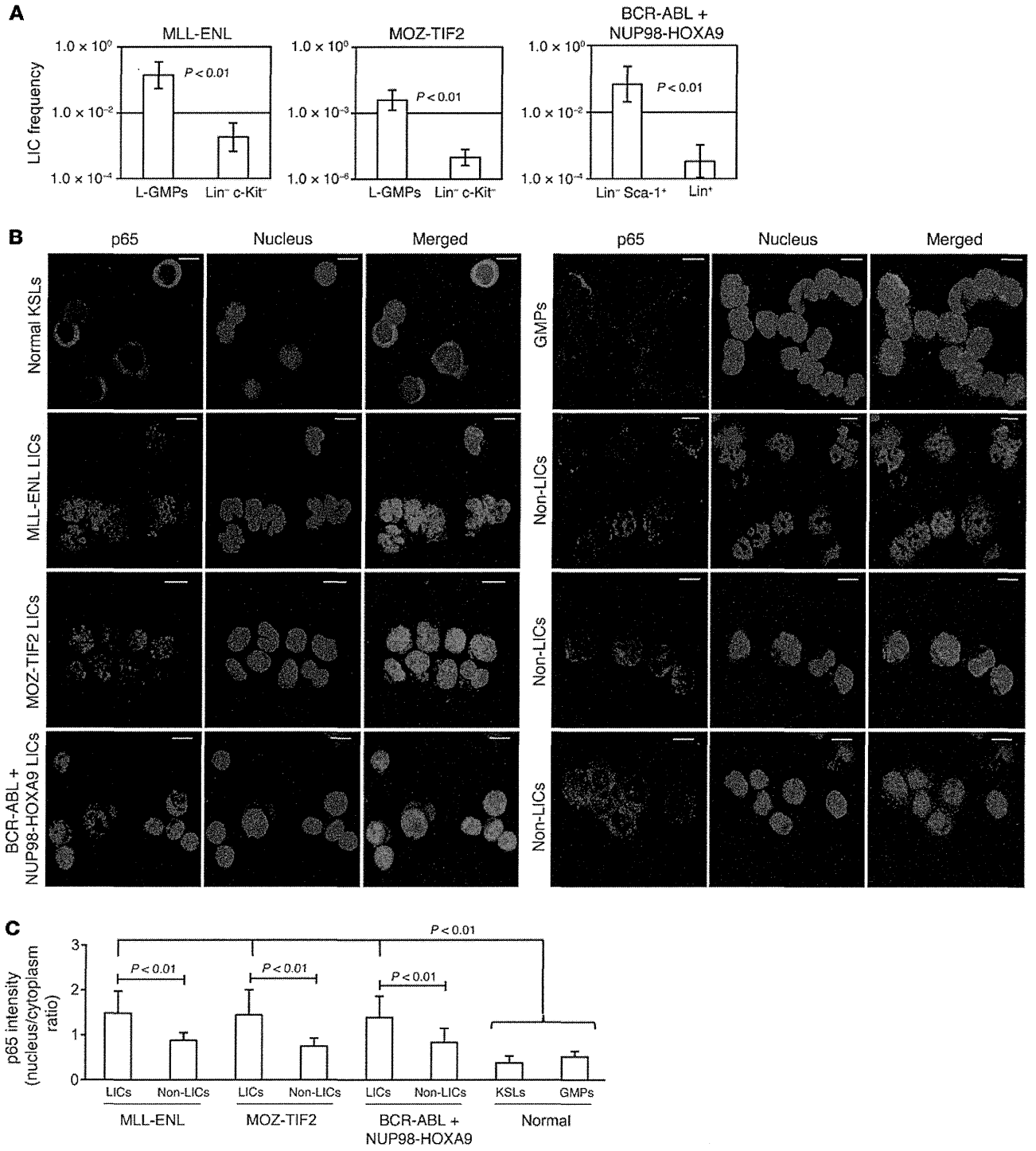

Figure 1

NF-κB pathway is activated in LICs of different murine myeloid leukemia models. (**A**) LIC frequency in the two fractions of each leukemia model as determined by limiting dilution assay. See Supplemental Table 1 for detailed transplantation results. (**B**) Immunofluorescence assessment for p65 nuclear translocation in KSLs, GMPs, LICs, and non-LICs in three leukemia models. Scale bars: 10 μm. (**C**) Quantification of p65 nuclear translocation assessed by the mean nucleus/cytoplasm intensity ratio. More than 50 cells were scored in each specimen, and the average intensity ratio with SD is shown.

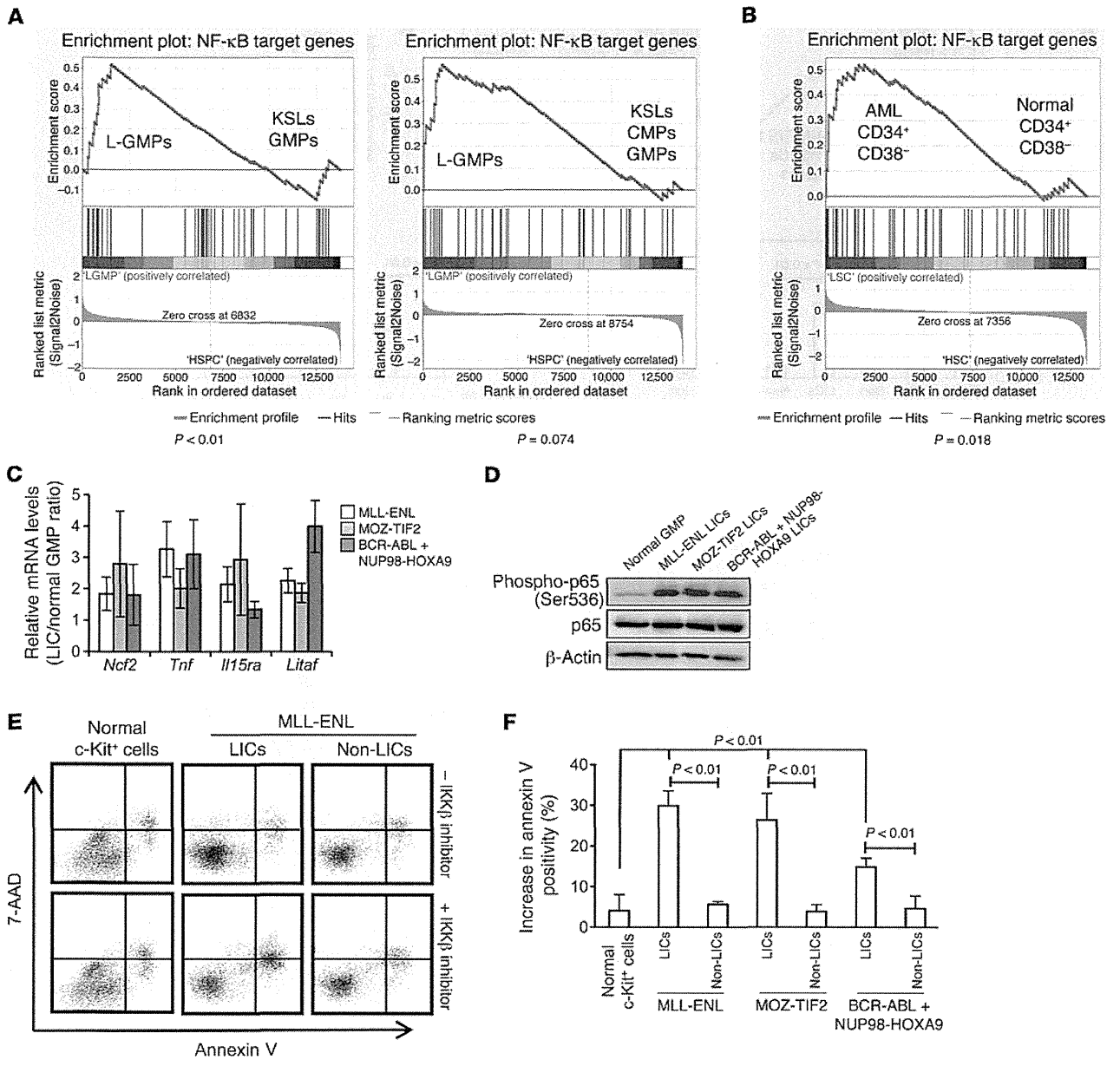

Figure 2

NF-κB transcription activity is increased in LICs. (**A**) GSEA of NF-κB target genes in the published gene expression data comparing LICs in leukemia mouse models with normal HSPCs. Left panel: comparison of MOZ-TIF2 L-GMP with normal KSLs and GMPs (GSE24797). Right panel: comparison of MLL-AF9 and HOXA9-MEIS1 L-GMPs with normal KSLs, common myeloid progenitors (CMPs), and GMPs (GSE20377). (**B**) GSEA of NF-κB target genes in $CD34^+CD38^-$ fractions in human AML versus healthy controls (GSE24006). (**C**) Quantitative real-time PCR analysis of a subset of NF-κB target genes in LICs of MLL-ENL, MOZ-TIF2, and BCR-ABL/NUP98-HOXA9 leukemia models relative to normal GMPs ($n = 4$). Error bars indicate SD. (**D**) Immunoblotting of total and phosphorylated p65 in normal GMPs and LICs in the three leukemia models. (**E**) Representative annexin V and 7-AAD profiles of normal c-Kit+ cells, L-GMPs, and $Lin^-c\text{-}Kit^-$ cells in MLL-ENL leukemic mice after a 24-hour culture with or without 10 μM IKK inhibitor (sc-514). (**F**) Average percentage increase in apoptotic cells in LICs of the three leukemia models compared with that in non-LICs and normal c-Kit+ cells treated with 10 μM IKK inhibitor (sc-514) ($n = 4$ each). Error bars indicate SD.

all three models (Figure 3, H and I). Interestingly, there was no significant difference in leukemogenicity among the recipient genotypes. These results indicate that autocrine TNF-α secretion is important for AML progression and that the contribution of paracrine effects derived from stromal cells is minimal.

The impact of specific NF-κB inhibition on leukemia progression. To investigate the influence of specific NF-κB pathway inhibition on leukemia progression in vivo, we transduced MLL-ENL leukemia cells with a retroviral vector expressing a dominant-negative form of IκBα (super repressor, referred to herein as IκB-SR) or

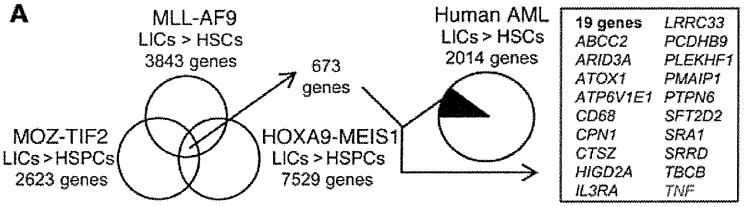

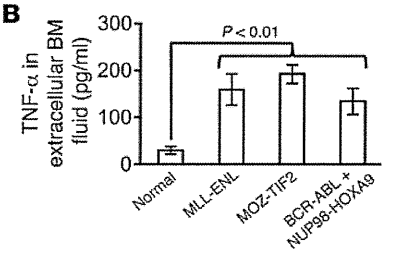

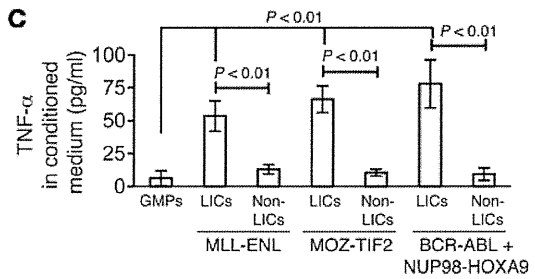

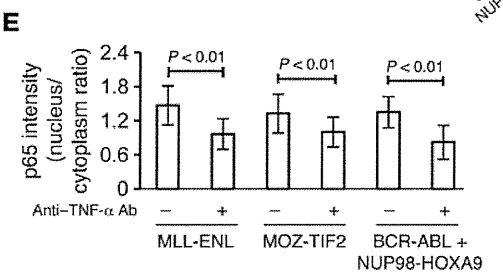

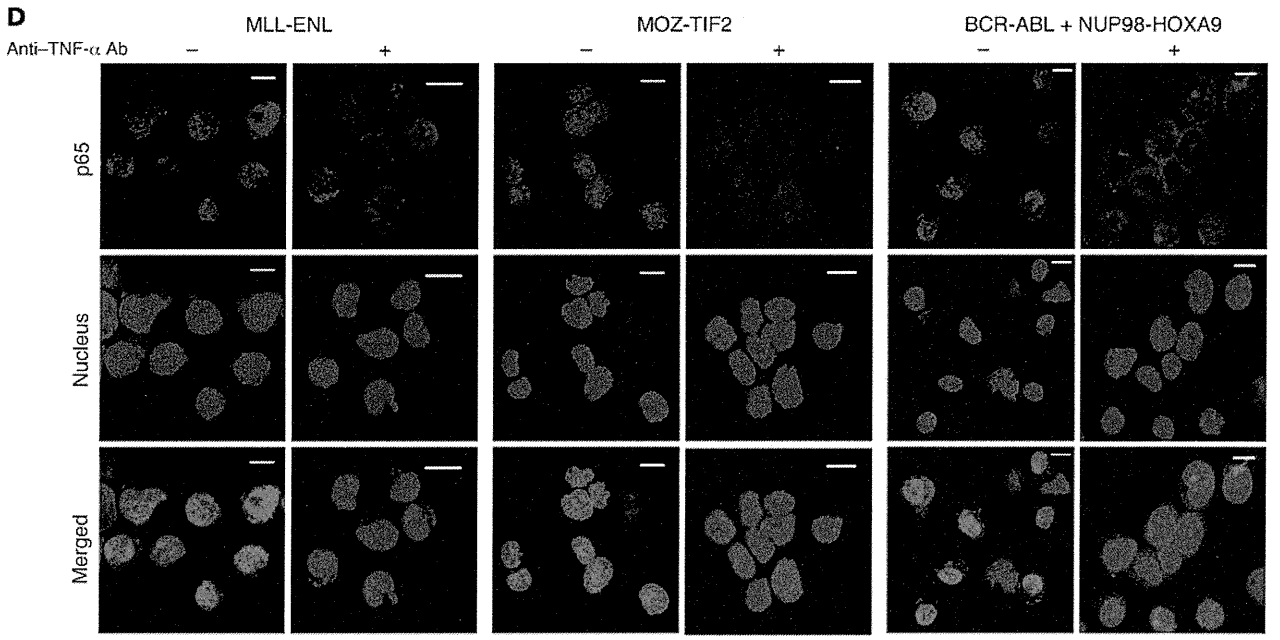

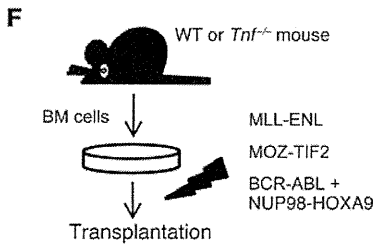

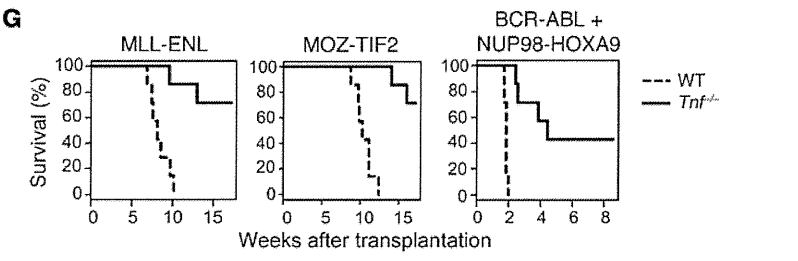

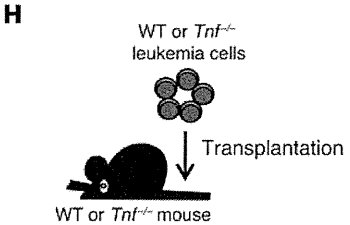

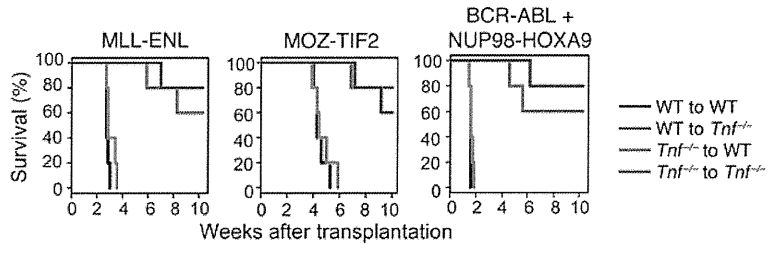

Figure 3
Autocrine TNF-α secretion maintains constitutive NF-κB activity and confers proliferative advantage in LICs. (**A**) Thorough investigation of genes with elevated expression in murine and human LICs compared with that in normal HSPCs in the published gene expression data. (**B**) TNF-α ELISA in extracellular fluid of normal or leukemic BM (n = 4 each). Error bars indicate SD. (**C**) TNF-α secretory ability in LICs compared with that of non-LICs and normal GMPs assessed by ELISA in cultured media (n = 4 each). Error bars indicate SD. (**D**) Immunofluorescence assessment for p65 nuclear translocation in LICs in serum-free culture medium with neutralizing antibody against TNF-α or isotype control. Scale bars: 10 μm. (**E**) Quantification of p65 nuclear translocation of LICs treated with neutralizing antibody against TNF-α or isotype control assessed by the mean nucleus/cytoplasm intensity ratio. More than 50 cells were scored in each specimen, and the average intensity ratio with SD is shown. (**F**) Schematic representation of the experiments. BM cells derived from WT or *Tnf*-knockout mice were transduced with MLL-ENL, MOZ-TIF2, and BCR-ABL plus NUP98-HOXA9 and transplanted into sublethally irradiated mice. (**G**) Survival curves of mice in the experiments shown in **F** (n = 7 each). (**H**) Schematic representation of the experiments. WT or $Tnf^{-/-}$ leukemia cells were secondarily transplanted into WT or $Tnf^{-/-}$ recipient mice. (**I**) Survival curves of mice in the experiments shown in **H** (n = 5 each).

with a control vector, transplanted them into recipient mice, and compared the characteristics of the repopulating cells (Figure 4A). Although the introduction of IκB-SR did not affect the morphology of MLL-ENL leukemia cells (Supplemental Figure 6A), p65 was almost completely sequestered in the cytoplasm of L-GMPs with IκB-SR (Figure 4B and Supplemental Figure 6B), and the expression levels of NF-κB target genes, including *Tnf*, were substantially decreased (Figure 4C). Considering that the blockage of autocrine TNF-α attenuated NF-κB signaling, we hypothesized that NF-κB activity and TNF-α secretion form a positive feedback loop in LICs. We therefore established MOZ-TIF2 and BCR-ABL/NUP98-HOXA9 leukemia cells with IκB-SR. The introduction of IκB-SR significantly decreased a proportion of the cells in the S and G2/M phases of the cell cycle and resulted in a substantial growth delay of those cells in liquid culture (Supplemental Figure 6, C and D). Moreover, leukemia cells with IκB-SR had a reduced colony-forming capacity, while the transduction of IκB-SR into normal HSCs had no significant influence on their colony-forming ability (Figure 4D). Finally, we transplanted leukemia cells with IκB-SR into sublethally irradiated mice and observed a remarkable delay in leukemia progression (Figure 4E). We also confirmed that the developed leukemia cells with IκB-SR had reduced nuclear translocation of p65 compared with that seen in control cells (Supplemental Figure 6E). In contrast, when normal BM cells were transduced with IκB-SR and transplanted into lethally irradiated mice, we observed no significant differences in the reconstitution capacity of the transplanted cells, nor did we find significant differences in peripheral blood cell counts or PBL surface-marker profiles, indicating that NF-κB pathway inhibition exerts a marginal influence on normal hematopoiesis (Supplemental Figure 7, A–C). Collectively, these findings clearly demonstrate that enhanced NF-κB activity in LICs plays a supportive role in leukemia progression and that NF-κB inhibition severely attenuates the proliferative ability of these cells.

To further validate the importance of the NF-κB pathway in leukemia progression, we used BM cells from $Rela^{flox/flox}$ mice (32). We similarly established leukemia cells derived from $Rela^{flox/flox}$ BM cells. Then, the developed leukemia cells were infected with codon-improved Cre recombinase–IRES-GFP (iCre-IRES-GFP) or GFP empty vector, and GFP-positive cells were isolated and secondarily transplanted into sublethally irradiated mice (Figure 4F). Remarkably, most of the mice transplanted with *Rela*-deleted leukemia cells did not develop leukemia (Figure 4G). Compared with controls, several mice did develop leukemia after longer latencies, but they did not develop leukemia after tertiary transplantation (data not shown), indicating that the complete ablation of NF-κB drastically reduced leukemogenicity.

High proteasome activity in LICs yields differences in NF-κB activity between leukemia cell populations. We next sought to elucidate the mechanisms underlying the differences in p65 nuclear translocation status between LICs and non-LICs. We confirmed that LICs had substantially lower IκBα protein levels compared with those of non-LICs in all three models (Figure 5, A and B). These results are very consistent with the p65 distribution status of LICs and non-LICs, considering that NF-κB is usually sequestered in the cytoplasm, bound to IκBα, and translocates to the nucleus, where IκBα is phosphorylated and degraded upon stimulation with a variety of agents such as TNF-α (33). We initially tested whether the expression of IκBα is downregulated in LICs at the transcription level and found that LICs had a tendency toward increased *Nfkbia* mRNA expression levels compared with non-LICs (Figure 5C). Moreover, when *Nfkbia* mRNA translation was inhibited by treatment with cycloheximide, the reduction in IκBα protein levels was more prominent in LICs than in non-LICs (Figure 5, D and E). These data indicate that the differences in IκBα levels are caused by the protein's predominant degradation in LICs. Since both LICs and non-LICs are similarly exposed to high levels of TNF-α within leukemic BM cells, we considered that there would be differences in response to the stimulus and sequentially examined the downstream signals. We first hypothesized that there is a difference in TNF-α receptor expression levels between LICs and non-LICs that leads to greater TNF-α signal transmission in LICs. The expression patterns of TNF receptors I and II were, however, almost similar in LICs and non-LICs, although they varied between leukemia models (Supplemental Figure 8A). We next tested the phosphorylation capacity of IκB kinase (IKK) by examining the ratio of phosphorylated IκBα to total IκBα after treatment with the proteasome inhibitor MG132. Contrary to our expectation, a similar accumulation of the phosphorylated form of IκBα was seen in both LICs and non-LICs, implying that they had no significant difference in IKK activity (Supplemental Figure 8B). Another possibility is that the differences in IκBα protein levels are caused by predominant proteasome activity in LICs, because it is required for the degradation of phosphorylated IκBα. We measured 20S proteasome activity in LICs and non-LICs in each leukemia model by quantifying the fluorescence produced upon cleavage of the proteasome substrate SUC-LLVY-AMC and observed a 2- to 3-fold higher proteasome activity in LICs (Figure 5F). Furthermore, the expression of several genes encoding proteasome subunits was elevated in LICs compared with that in non-LICs (Figure 5G). Similarly, the published gene expression data on human AML samples revealed that $CD34^+CD38^-$ cells had increased expression levels of proteasome subunit gene sets compared with those in $CD34^-$ cells (Supplemental Figure 9 and ref. 30). These findings suggest that enhanced proteasome activity in LICs leads to more efficient degradation of IκBα in response to TNF-α, thus resulting in elevated NF-κB activity. We then tested the effect of bortezomib, a well-

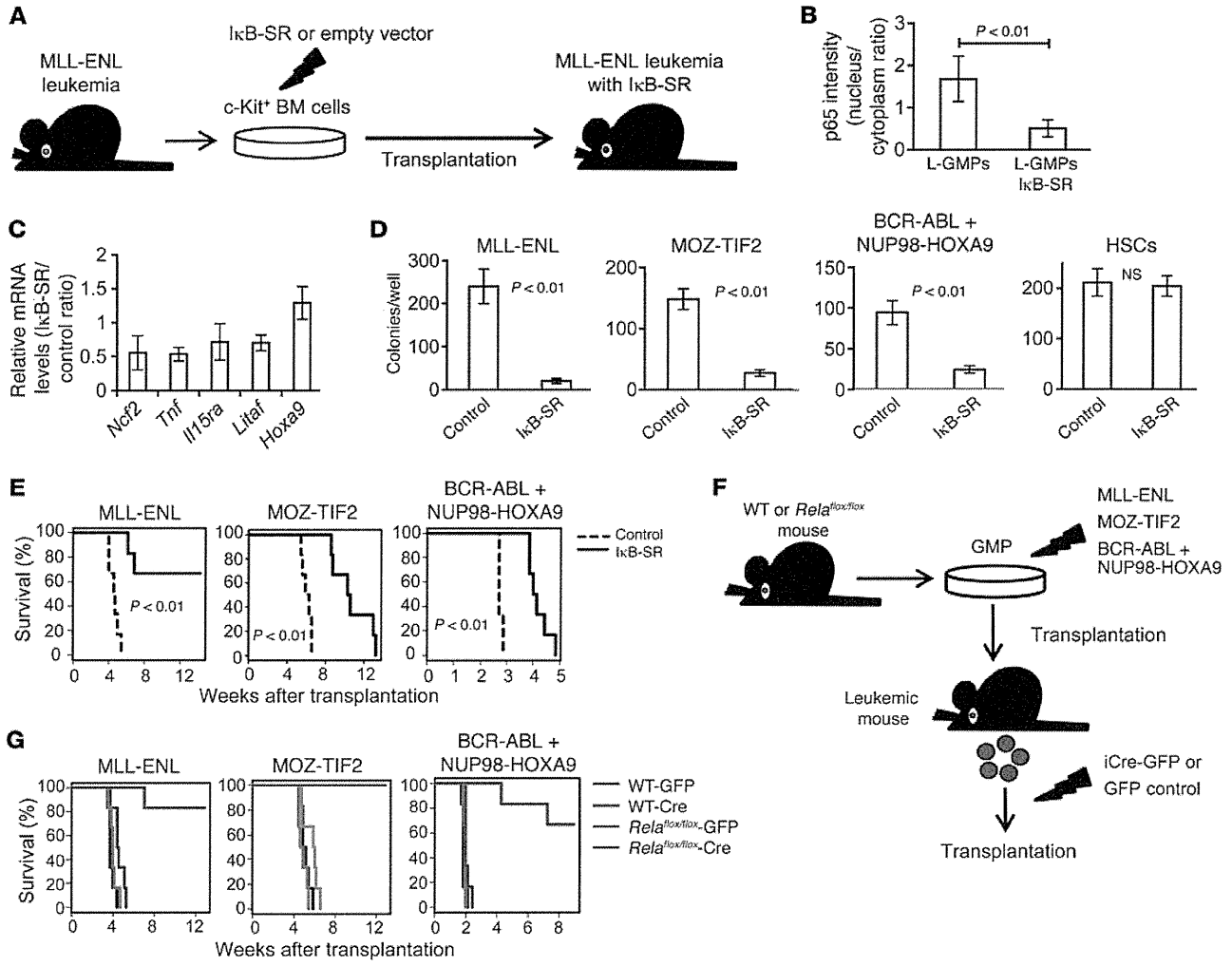

Figure 4

Specific inhibition of NF-κB significantly inhibits leukemia progression in vivo. (**A**) Schematic representation of the following experiments: c-Kit+ BM cells isolated from MLL-ENL leukemic mice were transduced with IκB-SR or control vector and transplanted into sublethally irradiated mice. (**B**) Quantification of p65 nuclear translocation assessed by the mean nucleus/cytoplasm intensity ratio by immunofluorescence staining. More than 50 cells were scored in each specimen, and the average intensity ratio with SD is shown. (**C**) Relative expression profiles of NF-κB target genes in MLL-ENL leukemia cells with or without IκB-SR. The change in *Hoxa9* expression is shown as a control gene not regulated by NF-κB. Error bars indicate SD ($n = 3$ each). (**D**) CFC assay of leukemia cells and normal HSCS with or without IκB-SR. Cells were seeded at 2,000 cells per well in MLL-ENL or BCR-ABL/NUP98-HOXA9–induced leukemia cells, at 500 cells per well in MOZ-TIF2–induced leukemia cells, and at 1,000 cells per well in normal HSCs ($n = 6$ in each experiment). (**E**) Survival curves of mice transplanted with MLL-ENL, MOZ-TIF2, and BCR-ABL/NUP98-HOXA9 leukemia cells with or without IκB-SR ($n = 6$ each). (**F**) Schematic representation of the following experiments: WT or *Rela*$^{flox/flox}$ mice were transduced with MLL-ENL, MOZ-TIF2, or BCR-ABL plus NUP98-HOXA9 and transplanted into sublethally irradiated mice. The developed leukemia cells were transduced with iCre-IRES-GFP or control GFP, and GFP+ cells were secondarily transplanted into mice. (**G**) Survival curves of mice in the experiments shown in **F** ($n = 6$ each).

known proteasome inhibitor, on LICs in vivo (Figure 5H). First, we treated mice with full-blown leukemia with a single injection of bortezomib and compared their BM surface-marker profiles with those of the vehicle-treated mice. Notably, bortezomib-treated mice showed a significant decrease in LIC-enriched populations in each type of leukemia (Figure 5, I and J). Finally, we treated mice with bortezomib after LIC transplantation and observed significant improvement in survival in those treated with bortezomib (Figure 5K). These results are very consistent with the selectively elevated proteasome activity we observed in LICs.

Enforced activation of the NF-κB pathway increases LIC frequency in leukemic BM. Given the supportive role of the NF-κB pathway in LIC proliferation as well as the differences in its activation status observed between LICs and non-LICs, we reasoned that the attenuation of NF-κB activity might be related to the transition from LICs to non-LICs. To test this hypothesis, we transduced MLL-ENL leukemia cells with a retrovirus encoding shRNA against IκBα and transplanted them into sublethally irradiated mice (Figure 6A). Because IκBα works as an inhibitor of NF-κB by holding it in the cytoplasm, its downregulation should function to

enhance NF-κB activity, regardless of the basal proteasome activity. We first confirmed that MLL-ENL leukemia cells with shRNA-mediated knockdown of IκBα (MLL-ENL-IκBα^{KD}) showed decreased IκBα protein levels in the cytoplasm and increased nuclear p65 protein levels, which would indicate that NF-κB signal was enhanced by the reduction of its cytoplasmic inhibitor (Figure 6B). In accordance with this finding, MLL-ENL-IκBα^{KD} cells had a significantly greater ability to secrete TNF-α than did control cells, reflecting an activated NF-κB/TNF-α signaling loop (Figure 6C). We further investigated the phenotype of leukemic mice with MLL-ENL-IκBα^{KD}. Interestingly, the BM of these MLL-ENL-IκBα^{KD} mice showed a marked increase in immature Gr-1^{lo} c-Kit^{hi} cell populations (Figure 6D). Consistent with this change, we found that these leukemic cells had a greater CFC capacity (Figure 6E). Additionally, in order to investigate the frequency of LICs in BM mononuclear cells, we performed limiting dilution analysis by secondary transplantation of leukemia cells. Although the disease latency for leukemia development was not significantly different among the leukemia cells, MLL-ENL-IκBα^{KD} leukemia cells had a marked abundance of LICs in the leukemic BM mononuclear cells compared with the control shRNA cells (Figure 6F and Supplemental Figure 10A). These data indicate that enforced NF-κB activation expands the LIC fraction in MLL-ENL leukemic BM cells. We also transduced normal BM cells with shRNAs against IκBα and transplanted them into lethally irradiated mice to test whether NF-κB activation by itself can induce leukemia or myeloproliferative-like disease. Over the 4-month follow-up period, the mice exhibited no significant change in peripheral blood values, indicating that NF-κB signal alone is not sufficient for leukemogenesis (Supplemental Figure 10B).

Significant correlation between NF-κB and TNF-α is observed in human AML LICs. Finally, we investigated NF-κB/TNF-α positive feedback signaling in human AML LICs. We analyzed CD34$^+$ CD38$^-$ cells derived from 12 patients with previously untreated or relapsed AML and the same cell population from 5 normal BM specimens (Table 1) and evaluated their NF-κB signal intensity. We also quantified the concentration of TNF-α in the culture media conditioned by CD34$^+$CD38$^-$ cells from each patient in order to measure the TNF-α secretory ability of these cells. As expected, our data from both of these analyses showed a wide variation among patients, one that might reflect a heterogeneous distribution and frequency of the LIC fraction in human AML cells, as was previously described (23). LICs in most of the patients did, however, show increased p65 nuclear translocation and TNF-α secretory potential compared with normal HSCs (Figure 7, A and B, and Supplemental Figure 11). We plotted these two parameters for each patient to compare between patients. Interestingly, a significant positive correlation was demonstrated statistically (P = 0.02), as LICS with enhanced p65 nuclear translocation showed a tendency toward abundant TNF-α secretion (Figure 7C). We also compared p65 intensity between LICs and non-LICs in 2 patients (patients 1 and 3) and found that p65 nuclear translocation was predominant in LICs, which is also consistent with the data obtained in murine AML cells (Supplemental Figure 11). Moreover, we cultured LICs with or without neutralizing antibodies against TNF-α and assessed p65 nuclear translocation to determine the effect of autocrine TNF-α on NF-κB activity. When incubated in the presence of TNF-α–neutralizing antibodies, nuclear translocation of p65 was significantly suppressed in LICs (Figure 7, D and E). These results support our hypothesis that a positive feedback loop exists between NF-κB and TNF-α in human AML LICs.

Discussion

In the present study, we provide evidence that LICs, but not normal HSPCs or non-LIC fractions within leukemic BM, exhibit constitutive NF-κB pathway activity in different types of myeloid leukemia models. Moreover, we identified the underlying mechanism involved in the maintenance of this pathway activity, which had yet to be elucidated. We found that autocrine TNF-α secretion, with the support of enhanced proteasome activity, contributed to a constitutive activation of the NF-κB pathway in LICs. Although we observed different sensitivities to the inhibition of these signaling cascades according to the type of leukemia, these cascades play an important role in LIC proliferation, especially considering that the complete ablation of *Tnf* or *Rela* distinctly suppressed leukemia progression in vivo. These findings, which we validated in human AML LICs, could translate into improved AML treatment strategies.

The strong connection between inflammation and cancer has been increasingly discussed, and the NF-κB pathway is now recognized as a major regulator bridging the two pathological conditions in different types of malignancies. In most of these malignancies, aberrant activation of the NF-κB pathway derives from inflammatory microenvironments that are mainly created by proinflammatory immune cells such as tumor-infiltrating macrophages, neutrophils, and lymphocytes (34, 35). In this study, however, LICs retained their p65 nuclear translocation even after serum-free culture, suggesting that the constitutive NF-κB activity of LICs is maintained in an autonomous fashion. Through our investigation of gene expression profiles in LICs and normal HSCs, we found that LICs had distinctly elevated TNF-α expression levels that contributed to the maintenance of NF-κB activation in LICs. Conversely, the introduction of IκB-SR markedly suppressed TNF-α expression levels, indicating that NF-κB activity and TNF-α secretion create a positive feedback loop in LICs. Moreover, our hypothesis is strongly supported by our findings that a positive correlation exists between NF-κB and TNF-α secretory activities in human AML CD34$^+$CD38$^-$ cells and that inhibition of autocrine TNF-α signaling attenuates p65 nuclear translocation. The role of TNF-α in the process of tumor promotion has recently been demonstrated in various types of solid tumors (36–39). It has also been reported that TNF-α is required for clonal evolution of myeloid malignancies (40). On the other hand, there has been controversy over the effect of TNF-α on leukemia cells when it was exogenously administered (41, 42). However, these previous studies did not address the critical question of whether endogenously secreted TNF-α is required for the maintenance of established leukemia cells, which is a crucially important aspect when considering therapeutic applications. We clearly reveal that the autonomously secreted TNF-α had beneficial effects on LIC proliferation through NF-κB activation, while the contribution of paracrine TNF-α secretion from BM microenvironments was minimal. Another important aspect of cytokine secretion by LICs that was not investigated in the present study is whether this secretion can exert some influence on BM stromal cells. Since the importance of bidirectional crosstalk between leukemia and niche cells through a variety of cytokines has increasingly been recognized (43), TNF-α secreted from LICs might also modulate the function of BM stromal cells, which could also have an impact on leukemia

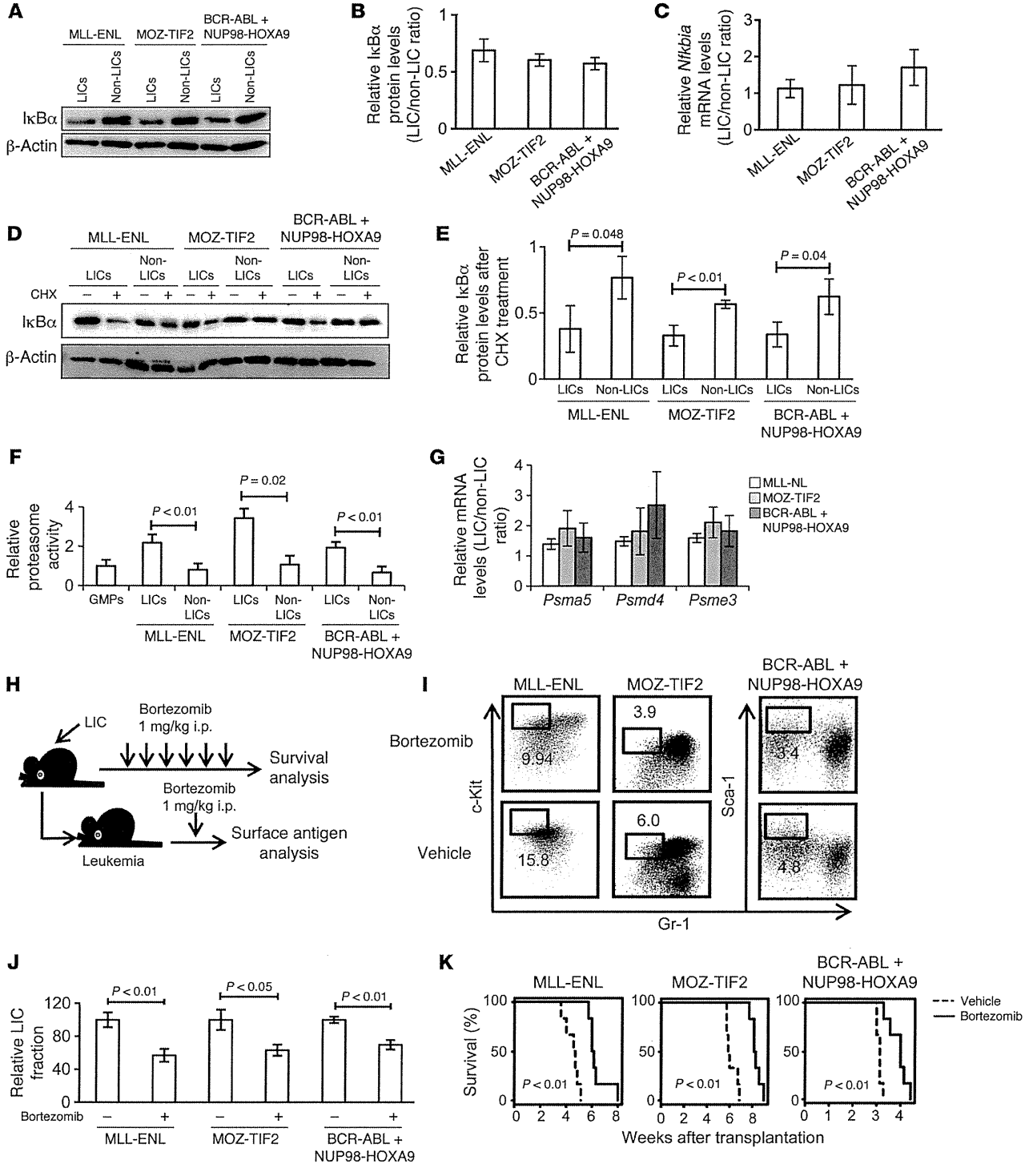

Figure 5
LICs have higher proteasome activity than non-LICs. (**A** and **B**) Immunoblotting of IκBα in LICs and non-LICs (**A**). Protein levels were quantified with ImageJ software (**B**). Data representative of four experiments with SD are shown. (**C**) Relative mRNA expression of *Nfkbia* in LICs compared with that in non-LICs ($n = 4$ each). Error bars indicate SD. (**D** and **E**) Immunoblotting of IκBα in LICs and non-LICs. Cells were pretreated with MG132 for 1 hour and incubated for an additional hour with or without cycloheximide (CHX) (**D**). IκBα protein levels were quantified with ImageJ software, and the relative decrease in IκBα after cycloheximide treatment was calculated ($n = 3$ each). Error bars indicate SD (**E**). (**F**) Analysis of 20S proteasome activity quantified with fluorescence produced upon cleavage of the proteasome substrate SUC-LLVY-AMC ($n = 4$ each). Error bars indicate SD. (**G**) Relative mRNA expression of proteasome subunits in LICs compared with that in non-LICs ($n = 4$ each). Error bars indicate SD. (**H**) Schematic representation of the experiments. Each type of LIC was secondarily transplanted into mice. Bortezomib was injected twice weekly or injected once after incidence of leukemia. (**I** and **J**) Comparison of surface marker profiles in leukemic mice treated with bortezomib or vehicle. Representative FACS data (**I**) and relative percentages of Gr-1^{lo} c-Kit^{hi} fraction in MLL-ENL– or MOZ-TIF2–induced leukemic mice, and Gr-1^{lo}Sca-1^{hi} fraction in BCR-ABL/NUP98-HOXA9–induced leukemic mice are shown ($n = 3$ each) (**J**). Values of control mice were normalized to 100%. Error bars indicate SD. (**K**) Survival curves of mice in the experiments shown in **H** ($n = 6$ each).

progression. Unveiling the role of TNF-α as a paracrine mediator would further extend the therapeutic options for AML.

Few studies have compared the NF-κB activity of different fractions within leukemia cells, and the mechanism underlying the difference in this activity has not been analyzed (44). We focused on proteasome activity as the essential machinery supporting NF-κB activity in LICs. Although high proteasome activity has been reported in various types of cancers (45, 46), its actual role in the malignant phenotype remained to be elucidated. In this study, we found that proteasome activity was especially high in LICs, which contributed to selective NF-κB activity in LICs via the efficient degradation of IκBα. Conversely, the inefficient NF-κB nuclear translocation we observed in non-LICs, despite TNF-α–enriched leukemic BM cells, could be explained by the low proteasome activity in these cells. Therefore, we postulate that both an activating stimulus such as TNF-α and high proteasome activity are required for efficient NF-κB signaling (Figure 7F). Both of these conditions are present exclusively in LICs, which acquire selective NF-κB activation. We also found that the expression levels of proteasome subunit genes were elevated in LICs compared with those in non-LICs, genes that could be involved in regulating proteasome function. Because we observed similar expression patterns in LICs and non-LICs in human AML cells, an elevated expression level of proteosome subunit genes might be one of the common characteristics of the LIC phenotype. Further studies will be needed to elucidate the regulatory mechanism of the proteasome gene families.

Our findings provide several advantages when considering their application to the clinical care setting. First, an activated NF-κB/TNF-α feedback loop was seen in AML LICs that had different genetic abnormalities. Although the therapeutic strategy of targeting aberrant molecules based on genetic abnormalities such as FLT3-ITD is promising, its application is limited to a particular group of patients. In contrast, inhibition of the NF-κB signal in addition to standard chemotherapy would show beneficial effects in most AML patients. Second, because there was a strong positive correlation between the NF-κB signal and TNF-α secretion, therapeutic efficacy could easily be inferred from the abundance of TNF-α instead of from evaluation of the activation status of NF-κB. Third, the NF-κB/TNF-α signal and enhanced proteasome activity are selectively seen in LICs, but not in normal HSCs. A recent study has shown that complete ablation of p65 in hematopoietic cells attenuates the long-term capacity for hematopoietic reconstitution (47). However, our data from the experiments in which we introduced IκB-SR into normal BM cells show that partial repression of NF-κB activity exerted minimal influence on normal hematopoiesis, while it markedly inhibited leukemia progression. These results indicate that there is a therapeutic window during which LICs can selectively be killed by NF-κB inhibition without seriously affecting normal hematopoiesis. Alternatively, there is some evidence that TNF-α has suppressive effects on normal HSCs (48, 49). The opposing role of TNF-α in LICs and HSCs is additionally beneficial, since anti–TNF-α therapy contributes to the recovery of normal hematopoiesis and attenuates LIC proliferation. Now that the TNF-α antagonist etanercept is widely used in inflammatory diseases such as rheumatoid arthritis, this drug might be a promising candidate for treating patients with AML.

In summary, the present study shows that blocking the NF-κB pathway offers a promising therapeutic approach for targeting LICs in various types of myeloid leukemia, without disturbing normal hematopoiesis. We further determined that autocrine TNF-α signaling and enhanced proteasome activity are crucial for maintaining constitutive NF-κB activity in LICs, findings that may also provide a new therapeutic opportunity.

Methods

Animals. C57BL/6 mice and BALB/c mice were purchased from Japan SLC, Inc. *Tnf*-knockout mice on a BALB/c background were established as described previously (50). *Rela*-floxed mice on a C57BL/6 background were provided by H. Algül and R.M. Schmid (32). BALB/c mice were used as the controls in the experiments using *Tnf*-knockout mice, and C57BL/6 mice were used in the other experiments.

Retrovirus production and BM transplantation assays. To obtain retrovirus supernatants, platinum-E (Plat-E) packaging cells were transiently transfected with each retrovirus vector, and the viral supernatants were collected 48 hours after transfection and used immediately for infection. To establish each myeloid leukemia mouse model, we used pMSCV-neo-MLL-ENL; pMSCV-MLL-ENL–internal ribosome entry site–*EGFP* (*IRES-EGFP*); pGCDNsam-MLL-ENL-*IRES*-Kusabira-Orange; pGCDNsam-MOZ-TIF2-*IRES-EGFP*; pGCDNsam-MOZ-TIF2-*IRES*-Kusabira-Orange; pGCDNsam-BCR-ABL-*IRES-EGFP*; pGCDNsam-BCR-ABL-*IRES*-Kusabira-Orange; and pMSCV-neo-NUP98-HOXA9. GMPs isolated from the BM of 8- to 10-week-old mice were transduced with the respective vectors and injected into sublethally irradiated (7.5 Gy) recipient mice. For experiments involving the generation of leukemia cells with IκB-SR, MLL-ENL leukemia cells were transduced with pBabe-GFP or pBabe-GFP-IκB-SR. MOZ-TIF2, and BCR-ABL/NUP98-HOXA9 leukemia cells were transduced with pGCDNsam-Kusabira-Orange or pGCDNsam-IκB-SR-IRES-Kusabira-Orange. For experiments involving the deletion of p65 in *Rela*-floxed mice, leukemia cells were established using Kusabira-Orange–containing retroviral vectors. The developed leukemia cells were transduced with pGCDNsam-EGFP or pGCDNsam-iCre-EGFP and transplanted into sublethally irradiated mice.

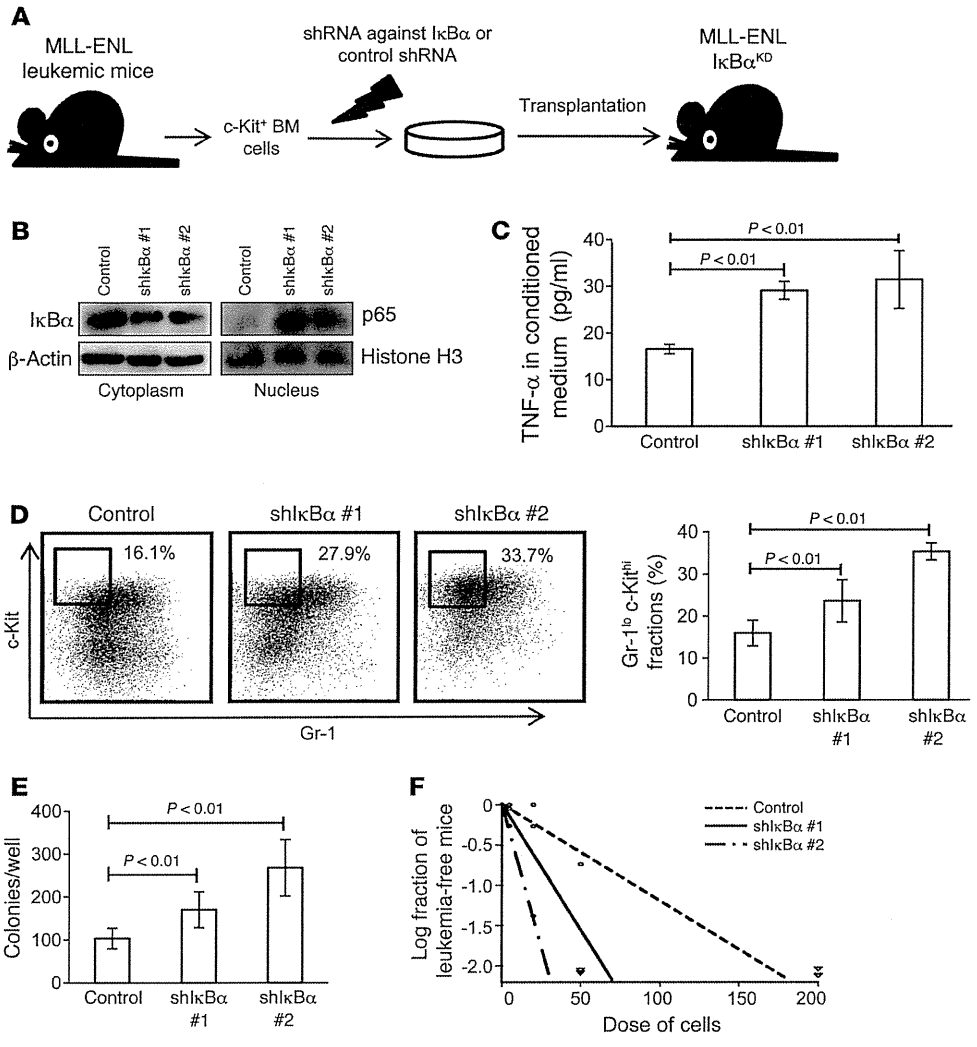

Figure 6
Forcible maintenance of NF-κB activity in leukemia cells enhances LIC frequency. (**A**) Schematic representation of the experiments. c-Kit+ BM cells isolated from MLL-ENL leukemic mice were transduced with shRNA against IκBα or control shRNA and transplanted into sublethally irradiated mice. (**B**) Immunoblotting of cytoplasmic IκBα and nuclear p65 in BM mononuclear cells from MLL-ENL-IκBα^{KD} mice compared with those from control leukemic mice. (**C**) TNF-α secretory ability of MLL-ENL-IκBα^{KD} leukemia cells compared with that of control leukemia cells (n = 4 each). Error bars indicate SD. (**D**) Surface marker profiles of MLL-ENL leukemic mice with or without knockdown of IκBα. Representative FACS plots and mean percentages of Gr-1^{lo}c-Kit^{hi} fractions (n = 6 each). (**E**) CFC assay of MLL-ENL leukemia cells with or without knockdown of IκBα (n = 6). Cells were seeded at 500 cells per well. Error bars indicate SD. (**F**) LIC frequency in BM mononuclear cells derived from MLL-ENL-IκBα^{KD} leukemic mice compared with those from control mice as determined by limiting dilution transplantation assay.

In vivo limiting dilution assays. Varying numbers of cells from different populations were transplanted into sublethally irradiated mice and monitored for disease development (see Supplemental Table 1 for the injected cell numbers).

Immunofluorescence and quantification of p65 nuclear translocation. A total of 1 × 10^4 to 5 × 10^4 cells were cytospun onto glass slides. The cells were fixed with 3.7% formaldehyde in PBS for 30 minutes, permeabilized by treatment with 0.2% Triton X in PBS for 10 minutes, and blocked with 1% BSA in PBS for 60 minutes. Then, the slides were incubated with rabbit anti-p65 polyclonal antibody (sc-372; 1:100 dilution; Santa Cruz Biotechnology Inc.) overnight at 4°C, followed by incubation with Alexa Fluor 555 goat anti-mouse IgG (1:250 dilution; Invitrogen) and TO-PRO3 (1:1,000 dilution; Invitrogen) for 90 minutes. For immunofluorescence staining of Kusabira-Orange$^+$ leukemia cells, Alexa Fluor 647 goat anti-mouse IgG (1:250 dilution; Invitrogen) was used as a secondary antibody, and the nucleus was stained with DAPI. After the cells were washed, they were treated with ProLong Gold Antifade Reagent (Invitrogen). Images were acquired using an Olympus FluoView FV10i confocal microscope with a ×60 objective oil immersion lens. The mean intensity of p65 in the nucleus and cytoplasm of each cell was measured within a region of interest (ROI) placed within the nucleus and cytoplasm. Similarly, the background intensity was quantified within an ROI placed outside the cells. All the measurements were performed using FluoView software. The background-subtracted intensity ratio of nucleus/cytoplasm was calculated in more than 50 cells in each specimen, and the average intensity with SD is presented.

Flow cytometry. Isolation of each fraction from normal or leukemic BM cells was performed using a FACSAria II (BD) cell sorter. For isolation of GMPs and KSLs, biotinylated antibodies against Gr-1 (RB6-8C5), CD11b (M1/70), B220 (RA-3-6B2), CD3 (145-2C11), CD4 (GK1.5), CD8 (53-6.7), and TER119 were used for lineage staining. A PerCP-Cy5.5–labeled streptavidin antibody was used for secondary staining, together with APC–anti–c-Kit (2B8), PE-Cy7–anti–Sca-1 (E13-161.7). FITC–anti-CD34 (RAM34), and PE–anti-CD16/32b antibodies (clone 93). The following antibodies were used for isolation of L-GMPs from GFP-containing leukemia cells: APC-Cy7–anti–streptavidin, PE-Cy5–anti–c-Kit (2B8), PE-Cy7–anti–Sca-1 (E13-161.7), Alexa Fluor 647–anti-CD34 (RAM34), and PE–anti-CD16/32b (clone 93). APC-antistreptavidin and PE-Cy7–anti–Sca-1 antibodies (E13-161.7) were used for sorting LICs and non-LICs in the BCR-ABL plus NUP98-HOXA9 leukemia model. See Supplemental Figures 1 and 2 for detailed FACS plots. For analysis of TNF receptor expression in leukemia cells, biotinylated antibodies against TNF receptor I or II (55R-170) and an APC-Cy7–antistreptavidin antibody were used. Analysis was performed using FlowJo software (Tree Star Inc.).

Table 1
Clinical characteristics of the 12 patients with AML and the 5 patients with normal BM findings

Patient no.	Age	Sex	BM findings	Disease status	Type	Cytogenetics	Blast (%)
1	42	M	AML	Untreated	M2	Normal	87
2	62	M	AML	Relapse	M1	47, XY, del(9)(q13q22),+10	96
3	69	M	AML	Untreated	M4	Normal	90
4	58	M	AML	Untreated	M3	46, XY, t(15;17)	63
5	75	M	AML	Untreated	M4	46, XY, inv(16)	27
6	62	F	AML	Untreated	AML-MRC	NA	24.8
7	72	F	AML	Untreated	AML-MRC	Complex	21
8	42	M	AML	Untreated	M4	46, XY, t(11;17)	25
9	66	M	AML	Untreated	M1	46, XY, t(8;21)	85.4
10	73	F	AML	Untreated	AML-MRC	Complex	44.5
11	65	M	AML	Untreated	AML-MRC	46, XY, t(1;3)	53.3
12	73	M	AML	Untreated	M2	46, XY, add(7)	51.5
13	67	F	Normal			Normal	
14	64	F	Normal			Normal	
15	47	F	Normal			Normal	
16	54	M	Normal			Normal	
17	29	M	Normal			Normal	

Real-time quantitative PCR. Real-time quantitative PCR was carried out on the LightCycler480 system (Roche) using SYBR green reagents according to the manufacturer's instructions. The results were normalized to *Gapdh* levels. Relative expression levels were calculated using the 2-ΔΔCt method (51). The following primers were used for real-time PCR experiments: *Gapdh* forward, TGGCCTCCAAGGAGTAAGAA, and reverse, GGTCTGGGATGGAAATTGTG; *Ncf2* forward, CCAGAAGACCTGGAATTTGTG, and reverse, AAATGCCAACTTTCCCTTTACA; *Tnf* forward, TCTTCTCATTCCTGCTTGTGG, and reverse, GGTCTGGGCCATAGAACTGA; *Il15ra* forward, TAAGCGGAAAGCTGGAACAT, and reverse, TGAGGTCACCTTTGGTGTCA; *Litaf* forward, CTCCAGGACCTTACCAAGCA, and reverse, AGGTGGATTCATTCCCTTCC; *Hoxa9* forward, GGTGCCTGCTGCAGTGTAT, and reverse, GTTCCAGCCAGGAGCGCATAT; *Psma5* forward, CGAGTACGACAGGGGTGTG, and reverse, TGGATGCCAATGGCTGTAG; *Psmd4* forward, GTACATGCGGAACGGAGACT, and reverse, TGTGGTCAGCACCTCACAGT; *Psme3* forward, TTTCAGAGAGCGGATCACAA, and reverse, GGTCATGGATATTTAGAATTGGTTC.

siRNA interference. Specific shRNAs targeting murine *Ikba* mRNA were designed and cloned into pSIREN-RetroQ-ZaGreen vectors. Control shRNA is a nonfunctional construct provided by Clontech. The target sequences, from 5′ to 3′, were: CCGAGACTTTCGAGGAAAT (shIκBα number 1), and AGCTGACCCTGGAAAATCT (shIκBα number. 2).

Immunoblotting. Membranes were probed with the following antibodies: anti-IκBα (Cell Signaling Technology), anti-phospho-IκBα (Ser32) (Cell Signaling Technology), anti-p65 (Santa Cruz Biotechnology Inc.), anti-phospho-p65 (Ser536) (Cell Signaling Technology), anti-β-actin (Cell Signaling Technology), and anti-histone H3 (Cell Signaling Technology). Protein levels were quantified with ImageJ software (NIH). To obtain nuclear and cytoplasmic extracts, an Active Motif Nuclear Extract Kit was used according to the manufacturer's instructions. Cycloheximide treatment assay was performed as described previously, with modification (52). Cells were pretreated with MG132 (20 μM) for 1 hour to initially inhibit the proteasomal degradation of IκBα. Cells were washed twice with medium, then cultured with or without 10 μg/ml of cycloheximide for an additional hour and harvested.

CFC assays. In each experiment, cells were plated onto MethoCult GF M3434 medium (STEMCELL Technologies). Colony numbers in each dish were scored on day 7.

Measurement of TNF-α levels in BM extracellular fluid and conditioned media. BM extracellular fluid was obtained by flushing bilateral femurs and tibia of individual mice with 400 μl PBS. The supernatant was collected after centrifugation. To obtain conditioned media, 0.3–1.0 × 10^6 murine leukemia cells or normal GMPs were cultured in RPMI medium containing 10% FBS and 10 ng/ml IL-3. After a 48-hour incubation, the culture supernatants were collected. The concentration of TNF-α was measured using a murine TNF-α ELISA kit (Gen-Probe Diaclone) according to the manufacturer's instructions. Similarly, 0.5 × 10^4 to 2.0 × 10^4 human AML or normal $CD34^+CD38^-$ cells were cultured for 48 hours in RPMI medium containing 10% FBS and 100 ng/ml SCF, IL-3, and thrombopoietin. The concentration of TNF-α in the harvested supernatants was measured with a human TNF-α Quantikine ELISA kit (R&D Systems).

20S proteasome activity. A 20S proteasome activity assay kit (Cayman Chemical) was used to analyze proteasome activity. A total of 5 × 10^4 freshly isolated normal GMPs, LICs, and non-LICs in each model were assayed according to the manufacturer's protocol. As a control, the proteasome activity of each cell was also assayed after the specific proteasome inhibitor epigallocatechin gallate was added. Fluorescence was measured with a Wallac ARVO V (PerkinElmer), and the proteasome activity of each cell type was calculated by subtracting the respective control value.

Bortezomib treatment studies. For in vivo treatment experiments, LICs of each leukemia model were injected into sublethally irradiated mice: 1 × 10^3 cells in the MLL-ENL or BCR-ABL/NUP98-HOXA9 models, and 1 × 10^4 cells in the MOZ-TIF2 model. Bortezomib was administrated i.p. at doses of 1.0 mg/kg twice weekly for 3 weeks. Treatment was started 1 week after transplantation in the MLL-ENL or BCR-ABL/NUP98-HOXA9 models, and 2 weeks after transplantation in the MOZ-TIF2 model. For experiments analyzing changes in LIC populations, bortezomib was administrated i.p. at doses of 1.0 mg/kg into fully developed leukemic mice. GFP^+ BM cells were collected 24 hours after injection, and surface marker profiles were analyzed.

Analysis of microarray data. We analyzed publicly available gene expression microarray data on murine and human samples from the Gene Expression Omnibus (GEO) database (GEO GSE24797, GSE20377, and GSE24006). A set of CEL files were downloaded from GEO and normalized using the JustRMA function from the Affy package 1.22.1 in Bioconductor. To compare expression profiles of the NF-κB target genes, normalized data were tested for GSEA using previously described NF-κB target gene sets (29), and a nominal *P* value was calculated. For screening of genes with elevated expression levels in LICs compared with those in normal HSPCs, the expression values of individual genes were compared between groups. Genes significantly elevated in LICs from all three leukemia models as determined by an unpaired Student's *t* test ($P < 0.05$)

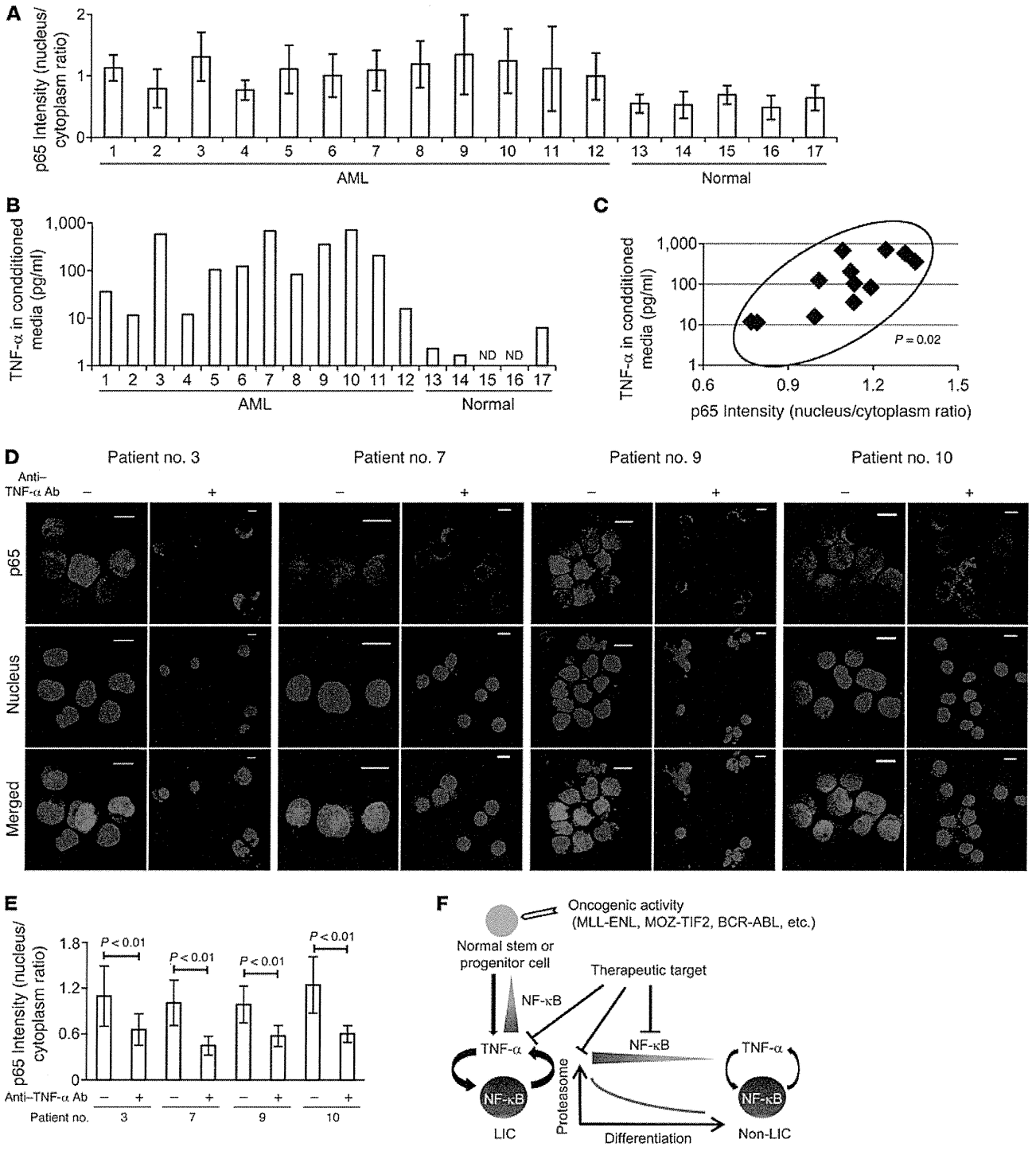

Figure 7

NF-κB/TNF-α positive feedback loop is activated in human AML LICs. (**A**) Quantification of p65 nuclear translocation assessed by the mean nucleus/cytoplasm intensity ratio by immunofluorescence staining. The CD34$^+$CD38$^-$ fractions isolated from AML or normal BM were analyzed. More than 50 cells were scored in each specimen, and the average intensity ratio with SD is shown. (**B**) TNF-α concentration of culture media conditioned by human AML LICs and normal HSCs measured by ELISA. ND, not detected. (**C**) Correlation between p65 nuclear translocation intensity ratio and TNF-α secretory ability of human AML LICs. (**D**) Immunofluorescence assessment of p65 nuclear translocation in LICs purified from 4 patients after serum-free culture with neutralizing antibody against TNF-α or isotype control. Scale bars: 10 μm. (**E**) Quantification of p65 nuclear translocation of LICs with or without neutralizing antibody against TNF-α assessed by the mean nucleus/cytoplasm intensity ratio. (**F**) Proposed model showing the role of NF-κB signaling in LICs. Positive feedback loop involving NF-κB/TNF-α promotes the maintenance and proliferation of LICs. The signaling is supported by active proteasome machinery, which declines with LIC differentiation.

were selected, among which genes also elevated in human AML LICs (Student's *t* test set at $P < 0.01$) were ultimately selected.

Statistics. Statistical significance of differences between groups was assessed with a 2-tailed unpaired Student's *t* test. Differences were considered statistically significant at a *P* value of less than 0.05. LIC frequency was calculated by Poisson statistics. In leukemia cell transplantation experiments, the overall survival of mice in BM transplantation assays is depicted by a Kaplan-Meier curve. Survival between groups was compared using the log-rank test. To measure the correlation between NF-κB intensity and TNF-α secretion in human AML samples, the Spearman's rank correlation coefficient was used.

Study approval. A total of 12 BM cells derived from patients with AML were obtained from the Department of Hematology and Oncology of the University of Tokyo Hospital. Five BM cells from patients diagnosed with lymphoid neoplasia without BM invasion were used as normal controls. The study was approved by the ethics committee of the University of Tokyo, and written informed consent was obtained from all patients whose samples were collected. All animal experiments were approved by the University of Tokyo Ethics Committee for Animal Experiments.

Acknowledgments

We thank T. Kitamura for the Plat-E packaging cells; H. Nakauchi and M. Onodera for the pGCDNsam-IRES-EGFP retroviral vector; R. Ono and T. Nosaka for the MLL-ENL cDNA; I. Kitabayashi for the MOZ-TIF2 cDNA; W. Hahn for the pBabe-GFP and pBabe-GFP-IκB-SR; and H. Algül and R.M. Schmid for providing the *Rela*-floxed mice. This work was supported by a Grant-in-Aid for Scientific Research A (KAKENHI 12020240) from the Ministry of Education, Culture, Sports, Science and Technology of Japan.

Received for publication December 3, 2012, and accepted in revised form October 17, 2013.

Address correspondence to: Mineo Kurokawa, Department of Hematology and Oncology, Graduate School of Medicine, The University of Tokyo, 7-3-1 Hongo, Bunkyo-ku, Tokyo 113-8655, Japan. Phone: 81.3.5800.9092; Fax: 81.3.5840.8667; E-mail: kurokawa-tky@umin.ac.jp.

1. Bonnet D, Dick JE. Human acute myeloid leukemia is organized as a hierarchy that originates from a primitive hematopoietic cell. *Nat Med.* 1997; 3(7):730–737.
2. Lapidot T, et al. A cell initiating human acute myeloid leukaemia after transplantation into SCID mice. *Nature.* 1994;367(6464):645–648.
3. Ishikawa F, et al. Chemotherapy-resistant human AML stem cells home to and engraft within the bone-marrow endosteal region. *Nat Biotechnol.* 2007; 25(11):1315–1321.
4. Marcucci G, Haferlach T, Döhner H. Molecular genetics of adult acute myeloid leukemia: prognostic and therapeutic implications. *J Clin Oncol.* 2011; 29(5):475–486.
5. Mardis ER, et al. Recurring mutations found by sequencing an acute myeloid leukemia genome. *N Engl J Med.* 2009;361(11):1058–1066.
6. Sen R, Baltimore D. Inducibility of kappa immunoglobulin enhancer-binding protein Nf-κB by a post-translational mechanism. *Cell.* 1986;47(6):921–928.
7. La Rosa FA, Pierce JW, Sonenshein GE. Differential regulation of the c-myc oncogene promoter by the NF-κB rel family of transcription factors. *Mol Cell Biol.* 1994;14(2):1039–1044.
8. Guttridge DC, Albanese C, Reuther JY, Pestell RG, Baldwin AS Jr. NF-κB controls cell growth and differentiation through transcriptional regulation of cyclin D1. *Mol Cell Biol.* 1999;19(8):5785–5799.
9. Duckett CS. Apoptosis and NF-κB: the FADD connection. *J Clin Invest.* 2002;109(5):579–580.
10. Karin M, Greten FR. NF-κB: linking inflammation and immunity to cancer development and progression. *Nat Rev Immunol.* 2005;5(10):749–759.
11. Karin M. Nuclear factor-κB in cancer development and progression. *Nature.* 2006;441(7092):431–436.
12. Pikarsky E, et al. NF-κB functions as a tumour promoter in inflammation-associated cancer. *Nature.* 2004;431(7007):461–466.
13. Guzman ML, et al. Nuclear factor-κB is constitutively activated in primitive human acute myelogenous leukemia cells. *Blood.* 2001;98(8):2301–2307.
14. Guzman ML, et al. Preferential induction of apoptosis for primary human leukemic stem cells. *Proc Natl Acad Sci U S A.* 2002;99(25):16220–16225.
15. Frelin C, et al. Targeting NF-κB activation via pharmacologic inhibition of IKK2-induced apoptosis of human acute myeloid leukemia cells. *Blood.* 2005;105(2):804–811.
16. Carvalho G, et al. Inhibition of NEMO, the regulatory subunit of the IKK complex, induces apoptosis in high-risk myelodysplastic syndrome and acute myeloid leukemia. *Oncogene.* 2007;26(16):2299–2307.
17. Guzman ML, et al. An orally bioavailable parthenolide analog selectively eradicates acute myelogenous leukemia stem and progenitor cells. *Blood.* 2007;110(13):4427–4435.
18. Jenkins C, et al. Nuclear factor-κB as a potential therapeutic target for the novel cytotoxic agent LC-1 in acute myeloid leukaemia. *Br J Haematol.* 2008;143(5):661–671.
19. Jin Y, et al. Antineoplastic mechanism of niclosamide in acute myelogenous leukemia stem cells: inactivation of the NF-κB pathway and generation of reactive oxygen species. *Cancer Res.* 2010;70(6):2516–2527.
20. Takahashi S, et al. Over-expression of Flt3 induces NF-κB pathway and increases the expression of IL-6. *Leuk Res.* 2005;29(8):893–899.
21. Liu S, et al. Sp1/NFκB/HDAC/miR-29b regulatory network in KIT-driven myeloid leukemia. *Cancer Cell.* 2010;17(4):333–347.
22. Nakagawa M, et al. AML1/RUNX1 functions as a cytoplasmic attenuator of NF-κB signaling in the repression of myeloid tumors. *Blood.* 2011; 118(25):6626–6637.
23. Eppert K, et al. Stem cell gene expression programs influence clinical outcome in human leukemia. *Nat Med.* 2011;17(9):1086–1093.
24. Sarry JE, et al. Human acute myelogenous leukemia stem cells are rare and heterogenous when assayed in NOD/SCID/IL2Rγc-deficient mice. *J Clin Invest.* 2011;121(1):384–395.
25. Liu T, et al. Functional characterization of meningioma 1 as collaborating oncogene in acute leukemia. *Leukemia.* 2010;24(3):601–612.
26. Kvinlaug BT, et al. Common and overlapping oncogenic pathways contribute to the evolution of acute myeloid leukemias. *Cancer Res.* 2011; 71(12):4117–4129.
27. Neering SJ, et al. Leukemia stem cells in a genetically defined murine model of blast-crisis CML. *Blood.* 2007;110(7):2578–2585.
28. Wang Y, et al. The Wnt/β-catenin pathway is required for the development ofleukemia stem cells in AML. *Science.* 2010;327(5973):1650–1653.
29. Hinz M, et al. Nuclear factor κB-dependent gene expression profiling of Hodgkin's disease tumor cells, pathogenetic significance, and link to constitutive signal transducer and activator of transcription 5a activity. *J Exp Med.* 2002;196(5):605–617.
30. Gentles AJ, Plevritis SK, Majeti R, Alizadeh AA. Association of a leukemic stem cell gene expression signature with clinical outcomes in acute myeloid leukemia. *JAMA.* 2010;304(24):2706–2715.
31. Kishore N, et al. A selective IKK-2 inhibitor blocks NF-κB-dependent gene expression in interleukin-1 β-stimulated synovial fibroblasts. *J Biol Chem.* 2003;278(35):32861–32871.
32. Algül H, et al. Pancreas-specific RelA/p65 truncation increases susceptibility of acini to inflammation-associated cell death following cerulein pancreatitis. *J Clin Invest.* 2007;117(6):1490–1501.
33. Beg AA, Finco TS, Nantermet PV, Baldwin AS Jr. Tumor necrosis factor and interleukin-1 lead to phosphorylation and loss of IκBα: a mechanism for NF-κB activation. *Mol Cell Biol.* 1993;13(6):3301–3310.
34. DeNardo DG, Coussens LM. Inflammation and breast cancer. Balancing immune response: crosstalk between adaptive and innate immune cells during breast cancer progression. *Breast Cancer Res.* 2007;9(4):212.
35. McLean MH, et al. The inflammatory microenvironment in colorectal neoplasia. *PLoS One.* 2011; 6(1):e15366.
36. Charles KA, et al. The tumor-promoting actions of TNF-α involve TNFR1 and IL-17 in ovarian cancer in mice and humans. *J Clin Invest.* 2009; 119(10):3011–3023.
37. Moore RJ, et al. Mice deficient in tumor necrosis factor-α are resistant to skin carcinogenesis. *Nat Med.* 1999;5(7):828–831.
38. Popivanova BK, et al. Blocking TNF-α in mice reduces colorectal carcinogenesis associated with chronic colitis. *J Clin Invest.* 2008;118(2):560–570.
39. Egberts JH, et al. Anti-tumor necrosis factor therapy inhibits pancreatic tumor growth and metastasis. *Cancer Res.* 2008;68(5):1443–1450.
40. Li J, et al. TNF-α induces leukemic clonal evolution ex vivo in Fanconi anemia group C murine stem cells. *J Clin Invest.* 2007;117(11):3283–3295.
41. Hoang T, Levy B, Ouetto N, Hainan A, Rodriguez-Cimadevilla JC. Tumor necrosis factor α stimulates the growth of the clonogenic cells of acute myeloblastic leukemia in synergy with granulocyte-macrophage colonystimulating factor. *J Exp Med.* 1989;170(1):15–26.
42. Khoury E, et al. Tumor necrosis factor alpha (TNF α) downregulates c-kit proto-oncogene product expression in normal and acute myeloid leukemia $CD34^+$ cells via p55 TNF alpha receptors. *Blood.* 1994;84(8):2506–2514.
43. Zhang B, et al. Altered microenvironmental regulation of leukemic and normal stem cells in chronic myelogenous leukemia. *Cancer Cell.* 2012; 21(4):577–592.
44. Kerbauy DM, Lesnikov V, Abbasi N, Seal S, Scott B, Deeg HJ. NF-κB and FLIP in arsenic trioxide (ATO)-induced apoptosis in myelodysplasticsyndromes (MDSs). *Blood.* 2005;106(12):3917–3925.
45. Adams J. The development of proteasome inhibitors as anticancer drugs. *Cancer Cell.* 2004;5(5):417–421.
46. Chen L, Madura K. Increased proteasome activity,

ubiquitin-conjugating enzymes, and eEF1A translation factor detected in breast cancer tissue. *Cancer Res.* 2005;65(13):5599–5606.
47. Stein SJ, Baldwin AS. Deletion of the NF-κB subunit p65/RelA in the hematopoietic compartment leads to defects in hematopoietic stem cell function. *Blood.* 2013;121(25):5015–5024.
48. Iversen PO, Wiig H. Tumor necrosis factor α and adiponectin in bone marrow interstitial fluid from patients with acute myeloidleukemia inhibit normal hematopoiesis. *Clin Cancer Res.* 2005; 11(19 pt 1):6793–6799.
49. Pronk CJ, Veiby OP, Bryder D, Jacobsen SE. Tumor necrosis factor restricts hematopoietic stem cell activity in mice: involvement of 2 distinct receptors. *J Exp Med.* 2011;208(8):1563–1570.
50. Taniguchi T, Takata M, Ikeda A, Momotani E, Sekikawa K. Failure of germinal center formation and impairment of response to endotoxin in tumor necrosis factor alpha-deficient mice. *Lab Invest.* 1997; 77(6):647–658.
51. Schmittgen TD, Livak KJ. Analyzing real-time PCR data by the Comparative C(T) method. *Nat Protoc.* 2008;3(6):1101–1108.
52. Jain AK, Bloom DA, Jaiswal AK. Nuclear import and export signals in control of Nrf2. *J Biol Chem.* 2005;280(32):29158–29168.

nature COMMUNICATIONS

ARTICLE

Received 29 Jan 2014 | Accepted 21 Jul 2014 | Published 27 Aug 2014

DOI: 10.1038/ncomms5770

Recurrent *CDC25C* mutations drive malignant transformation in FPD/AML

Akihide Yoshimi[1,*], Takashi Toya[1,*], Masahito Kawazu[2], Toshihide Ueno[3], Ayato Tsukamoto[1], Hiromitsu Iizuka[1], Masahiro Nakagawa[1], Yasuhito Nannya[1], Shunya Arai[1], Hironori Harada[4], Kensuke Usuki[5], Yasuhide Hayashi[6], Etsuro Ito[7], Keita Kirito[8], Hideaki Nakajima[9], Motoshi Ichikawa[1], Hiroyuki Mano[3] & Mineo Kurokawa[1]

Familial platelet disorder (FPD) with predisposition to acute myelogenous leukaemia (AML) is characterized by platelet defects with a propensity for the development of haematological malignancies. Its molecular pathogenesis is poorly understood, except for the role of germline *RUNX1* mutations. Here we show that *CDC25C* mutations are frequently found in FPD/AML patients (53%). Mutated CDC25C disrupts the G2/M checkpoint and promotes cell cycle progression even in the presence of DNA damage, suggesting a critical role for CDC25C in malignant transformation in FPD/AML. The predicted hierarchical architecture shows that *CDC25C* mutations define a founding pre-leukaemic clone, followed by stepwise acquisition of subclonal mutations that contribute to leukaemia progression. In three of seven individuals with *CDC25C* mutations, *GATA2* is the target of subsequent mutation. Thus, *CDC25C* is a novel gene target identified in haematological malignancies. *CDC25C* is also useful as a clinical biomarker that predicts progression of FPD/AML in the early stage.

[1] Department of Hematology and Oncology, Graduate School of Medicine, The University of Tokyo, 7-3-1 Hongo, Bunkyo-ku, Tokyo 113-8655, Japan. [2] Department of Medical Genomics, Graduate School of Medicine, The University of Tokyo, 7-3-1 Hongo, Bunkyo-ku, Tokyo 113-8655, Japan. [3] Department of Cellular Signaling, Graduate School of Medicine, The University of Tokyo, 7-3-1 Hongo, Bunkyo-ku, Tokyo 113-8655, Japan. [4] Department of Hematology, Juntendo University School of Medicine, 3-1-3 Hongo, Bunkyo-ku, Tokyo 113-8431, Japan. [5] Department of Hematology, NTT Medical Center Tokyo, 5-9-22 Higashi-Gotanda, Shinagawa-ku, Tokyo 141-8625, Japan. [6] Department of Hematology/Oncology, Gunma Children's Medical Center, 779 Simohakoda, Kitaakebonocho, Shibukawa-shi, Gunma 377-8577, Japan. [7] Department of Pediatrics, Graduate School of Medicine, Hirosaki University, 53 Honmachi, Hirosaki-shi, Aomori 036-8563, Japan. [8] Department of Hematology and Oncology, University of Yamanashi, 1110 Simokawakita, Chuou-shi, Yamanashi 409-3898, Japan. [9] Division of Hematology, Department of Internal Medicine, Keio University School of Medicine, 35 Shinanomachi, Shinjyuku-ku, Tokyo 160-8582, Japan. * These authors contributed equally to this work. Correspondence and requests for materials should be addressed to M.K. (email: kurokawa-tky@umin.ac.jp).

Familial platelet disorder (FPD)/acute myelogenous leukaemia (AML) (MIM601399) is an autosomal dominant disorder with inherited thrombocytopenia, abnormal platelet function and a lifelong risk of the development of a variety of haematological malignancies[1], such as AML, myelodysplastic syndromes (MDS) and myeloproliferative neoplasms. Although inherited *RUNX1* mutations are the cause of the congenital thrombocytopenia, it remains unclear whether a mutation in *RUNX1*, which is generally known to have a dominant-negative effect[2–4], is sufficient to induce the development of haematological malignancies in individuals with FPD/AML. It is also not known whether additional gene mutations are required for the transformation, and, if so, which genes are involved. Given that only 40% of FPD/AML patients develop these neoplasms[5] and that a relatively long period is required for subsequent *RUNX1* mutation-mediated development of neoplasms in FPD/AML, the secondary genetic events may function as a driver to promote malignant transformation. We reasoned that identifying gene mutations responsible for the malignant transformation of FPD/AML would provide indispensable information for addressing these questions. However, only about 30 pedigrees with FPD/AML have been reported so far, and the rarity of this disorder has impeded the establishment of clinical diagnostic criteria and the clinical improvement to refine cancer therapy and to identify biomarkers that would allow detection of patients at risk for the onset of malignancies in FPD/AML.

We collected DNA samples and clinical information of 73 individuals, belonging to 57 pedigrees, who have a history of familial thrombocytopenia and/or haematological malignancies, with the aim of identifying pedigrees with FPD/AML and uncovering recurrent mutations that drive the malignant transformation. Next-generation sequencing and single-cell sequencing strategy suggest that somatic mutation in *CDC25C* may be one of the early genetic events for leukaemic initiation in FPD/AML, and further stepwise acquisition of mutations such as *GATA2* leads to FPD/AML-associated leukaemic progression. These observations shed light on a part of leukemogenesis in FPD/AML.

Results

A novel gene target in haematological disorders. Thirteen patients in 7 pedigrees were diagnosed as having FPD/AML after screening for germline *RUNX1* mutations in 73 index patients; 7 of the 13 patients had developed haematological malignancies, while the other 6 only showed thrombocytopenia (Table 1). Most of the detected *RUNX1* mutations were point mutation in Runt homology domain or frame-shift mutation that lost transactivation domain, consistent with the previous reports[2,4]. As haploinsufficiency of *RUNX1* might cause familial thrombocytopenia with propensity to develop AML[1], we also examined whether the pedigrees have *RUNX1* loss of heterozygosity (LOH) or not. A synchronized quantitative-PCR method[6] and single-nucleotide polymorphism (SNP) sequencing detected no case with LOH in *RUNX1* in our cohort (Supplementary Fig. 1 and detailed in Methods). To systematically identify additional genetic alterations, we utilized whole-exome sequencing for two individuals from the same FPD/AML pedigree who shared a common *RUNX1*_p.Phe303fs mutation and who had developed MDS (subject 20) or myelofibrosis (subject 21) at the age of 37 and 17 years, respectively. In both these patients, the disease had progressed to AML[7]. Validation by Sanger sequencing and/or targeted deep sequencing of candidate mutations in paired tumour/normal DNA samples confirmed 10 (subject 20) and 8 (subject 21) somatically acquired nonsynonymous mutations (Table 2; Supplementary Figs 2–4; Supplementary Methods). Surprisingly, both patients carried the identical somatic *CDC25C* mutation (p.Asp234Gly), which had not been reported previously in human cancers (Fig. 1a,b). Prompted by this finding, we investigated *CDC25C* mutations in other FPD/AML cases by deep sequencing. In total, four of seven affected patients with haematological malignancies had *CDC25C* mutations, of which three carried the same p.Asp234Gly mutation. Moreover, *CDC25C* mutations were detected in an additional three FPD/AML patients who had not yet developed haematological malignancies, although the variant allele fractions (VAFs) were much lower in this group of patients than in those who had already developed haematological malignancies (Fig. 1c; Table 1). Thus, 7 of the 13 FPD/AML patients (53%) harboured a *CDC25C* mutation. *CDC25C* was also screened for mutations in 90 sporadic MDS and 53 AML patients, including 13 MDS and 3 AML cases who carried *RUNX1* mutations. No *CDC25C* mutations were identified in the 90 sporadic cases, except for the p.Ala344Val in an MDS patient bearing a *RUNX1* mutation, indicating that *CDC25C* mutations were significantly associated with germline, but not with somatic *RUNX1* mutations ($P = 0.004$; Supplementary Fig. 5; Supplementary Table 1).

Clonal evolution of FPD/AML. Deep sequencing of individual mutations that had been detected by whole-exome sequencing

Table 1 | Mutational status of *CDC25C* in FPD/AML patients.

Pedigree number	Subject number	RUNX1 mutation	Disease status	Age, years*	CDC25C mutation	VAF (%)
18	20	p.Phe303fs	MDS/AML	37/38	p.Asp234Gly	31.7/45.8
	21		MF/AML	17/18	p.Asp234Gly	31.1/39.0
19	22	p.Arg174*	AML	41	p.His437Asn	39.7
54	65	p.Ser140Asn	MDS	25	—	—
	66		AML	56	p.Asp234Gly	24.2
32	38	p.Leu445Pro	HCL	72	—	—
16	18	p.Thr233fs	Thrombocytopenia	—	p.Asp234Gly	5.9
53	62	p.Gly262fs	MDS	12	—	—
	63		Thrombocytopenia	—	—	—
	67		Thrombocytopenia	—	—	—
57	71	p.Gly172Glu	Pancytopenia†	—	p.Asp234Gly	8.3
	72		Thrombocytopenia	—	—	—
	73		Thrombocytopenia	—	p.Lys233Glu	1.8

AML, acute myeloid leukemia; FPD, familial platelet disorder; HCL, hairy cell leukemia; MDS, myelodysplastic syndrome; MF, myelofibrosis; VAF, variant allele fraction.
*Age at the time of diagnosis of each haematological malignancy is shown.
†Thrombocytopenia, leukopenia and iron-deficiency anemia were diagnosed.

Table 2 | Validated somatic mutations.

Gene symbol	Ref seq_no.	Amino-acid change	Position (hg19)	Base change	Mutation type	SIFT prediction	VAF at MDS/MF (%)	VAF at AML (%)
Subject 20								
AGAP4	NM_133446	p.Arg484Cys	g.chr10:46321905	C->T	Missense	Damaging	13.2	11.5
CDC25C	NM_001790	p.Asp234Gly	g.chr5:137627720	A->G	Missense	Damaging	31.7	45.8
CHEK2	NM_007194	p.Arg406His	g.chr22:29091740	G->A	Missense	Tolerated	14.6	11.1
COL9A1	NM_001851	p.Gly878Val	g.chr6:70926733	G->T	Missense	Damaging	9.6	26.4
DTX2	NM_001102594	p.Pro74Arg	g.chr7:76110047	C->G	Missense	Damaging	18.3	11.2
FAM22G	NM_001170741	p.Ser508Thr	g.chr9:99700727	T->A	Missense	Tolerated	10.2	27.6
GATA2	NM_001145661	p.Leu321His	g.chr3:128202758	T->A	Missense	Damaging	0.0	28.1
LPP	NM_001167671	p.Val538Met	g.chr3:188590453	G->A	Missense	Damaging	9.7	28.8
RP1L1	NM_178857	p.Ser215fs	g.chr8:10480295	insC	Frameshift	Damaging	14.2	12.7
SIGLEC9	NM_014441	p.Ser437Gly	g.chr19:51633253	A->G	Missense	Tolerated	27.4	42.5
Subject 21								
ANXA8L1	NM_001098845	p.Val281Ala	g.chr10:48268018	T->C	Missense	Damaging	30.8	36.8
CDC25C	NM_001790	p.Asp234Gly	g.chr5:137627720	A->G	Missense	Damaging	31.1	39.1
DENND5A	NM_001243254	p.Arg320Ser	g.chr11:9215218	A->C	Missense	Damaging	29.5	37.3
FER	NM_005246	p.Tyr634Cys	g.chr5:108382876	A->G	Missense	Damaging	1.4	30.4
FNDC1	NM_032532	p.Arg189Cys	g.chr6:159636081	C->T	Missense	Damaging	29.3	35.9
OR8U1	NM_001005204	p.Asn175Ile	g.chr11:56143623	A->T	Missense	Damaging	30.0	34.1
PIDD	NM_145886	p.Arg342Cys	g.chr11:802347	C->T	Missense	Damaging	3.3	28.3
ZNF614	NM_025040	p.Glu202Gly	g.chr19:52520246	A->G	Missense	Damaging	28.7	33.7

AML, acute myeloid leukemia; MDS, myelodysplastic syndrome; MF, myelofibrosis; SIFT, sorting intolerant from tolerant; VAF, variant allele fraction.

allowed accurate determination of their VAFs; on this basis, we could establish an inferred model of clonal evolution in terms of individual mutations in subjects 20 and 21 (Fig. 2a,b; Supplementary Fig. 6a,b). Intratumoral heterogeneity was evident at both MDS and AML phases in subject 20. According to the predicted model, a founding clone with a *CDC25C* mutation acquired additional mutations in *COL9A1*, *FAM22G* and *LPP* (group A), followed by the emergence of a *GATA2* mutation (group B), which was associated with leukaemic transformation, whereas the size of another subclone, defined by mutations in *CHEK2* and three other genes (group C), was unchanged. To validate this hierarchical model, single-cell genomic sequencing was performed using genomic DNA of 63 bone marrow cells from subject 20 when the patient was in the AML phase. Assuming that all cells harbour the *RUNX1* mutation, the false-negative rate of the procedure reached 35%, possibly due to biased allele amplification (Online Methods). However, this technique successfully demonstrated that the group A/B and group C mutations were mutually exclusive (Fig. 2c; Supplementary Table 2). To statistically evaluate this possibility, we assumed two hypotheses (H_0: the mutational status of genes in group A/B and group C is independent; H_1: mutations in group A/B and group C are mutually exclusive) and calculated each probability distribution (P_i: probability that the current results as shown in Fig. 2c were obtained under the hypothesis H_i). Our mutational profile data were achieved with a much higher likelihood under H_1 than H_0 (Supplementary Fig. 7 and detailed in Supplementary Methods). Similarly, the clonal architecture for subject 21 was portrayed in Fig. 2b and Supplementary Fig. 6b. In both scenarios, *CDC25C* mutations seemed to represent a founding mutation with the highest VAF, suggesting that the *CDC25C* mutation contributed to the establishment of a founding tumour population as an early genetic event, whereas progression to AML seemed to be accompanied by the appearance of additional mutations, indicating a multistep process in leukemogenesis.

Along with the somatic mutations found in subjects 20 and 21, a *GATA2* mutation was also identified in subject 22 (Fig. 3a). This patient developed AML with multilineage dysplasia, which led to the diagnosis of AML – MRC (myelodysplasia-related changes). Remission-induction therapies were only partially effective and the blast cell count was reduced from 54 to 5.6%, while dysplastic features persisted (Fig. 3b; Supplementary Fig. 8). Allogeneic stem cell transplantation was successfully performed from a human leukocyte antigen-matched unrelated donor and durable complete remission, with 100% donor chimerism, was achieved. During treatment, the VAF of the *GATA2* mutation decreased virtually in parallel with the blast cell percentage, while the VAF of the *CDC25C* mutation hovered at a high level before transplantation. Thus, we hypothesized that the *GATA2* mutation induced leukaemia progression in this patient, whereas the *CDC25C* mutation was associated with the pre-leukaemic status. Another *GATA2* mutation (p.Leu359Val) was found in subject 18, with a VAF (0.94%), who showed only thrombocytopenia without any signs of leukaemia progression and who had a small subclone with a concurrent *CDC25C* mutation (Fig. 3c). Although *GATA2* mutations are detected in a small number of patients with FPD/AML, the findings described above suggest that mutation of *GATA2* is a key factor promoting disease progression in FPD/AML (Fig. 3d).

Biological consequences of *CDC25C* mutations. We next investigated the possible impact of *CDC25C* mutation on clonal selection and evolution. CDC25C is a phosphatase that prevents premature mitosis in response to DNA damage at the G2/M checkpoint, while it is constitutively phosphorylated at Ser216 throughout interphase by c-TAK1 (refs 8–10). When phosphorylated at Ser216, CDC25C binds to 14-3-3 protein[11], leading to sequestration of CDC25C to the cytoplasm and its inactivation. Ba/F3 cells were transduced with retroviruses encoding the wild-type or mutant CDC25C containing each of the individual mutations (p.Asp234Gly, p.Ala344Val, p.His437Asn and p.Ser216Ala), and assayed for the phosphorylation status, 14-3-3 protein-binding capacity and intracellular localization of each of these proteins. The Ser216Ala mutant form

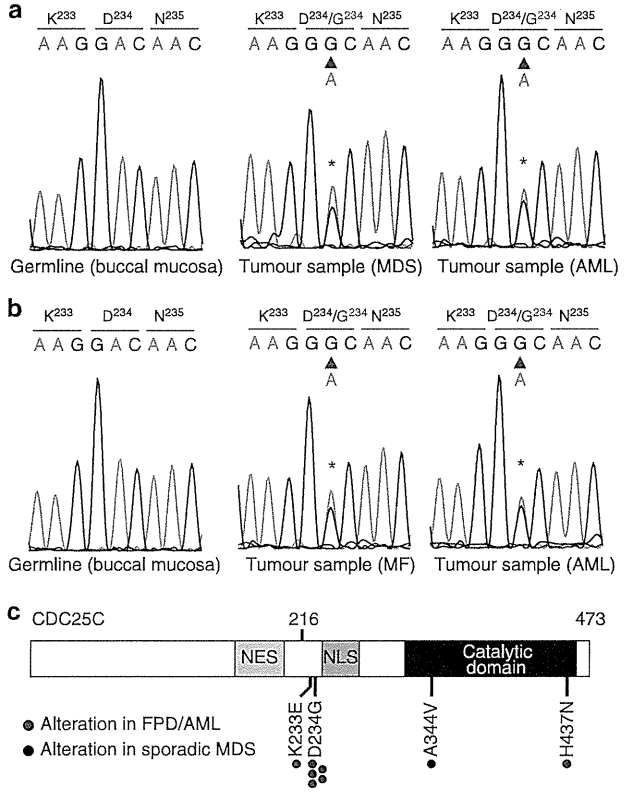

Figure 1 | Mutation in *CDC25C* recurs in cases of FPD/AML. (**a**,**b**) Sanger sequencing of *CDC25C* mutations found in whole-exome sequencing is shown. Both forward and reverse traces were available for each mutation, but only one trace is shown above. The results of buccal mucosa, pre-leukaemic phase and leukaemic phase is demonstrated for subject 20 (**a**) and subject 21 (**b**), respectively. (**c**) The distribution of alterations is shown for the CDC25C protein. NES, a putative nuclear export signal domain between amino acids 177–200; NLS, a putative nuclear localization sequence domain consisting of amino acids 240–244.

of CDC25C, which lacks the phosphorylation site, was used as a negative control. In all of the mutated forms of CDC25C, the capacity for binding to c-TAK1 was reduced (Fig. 4a,b; Supplementary Fig. 9a,b), resulting in decreased phosphorylation of CDC25C at Ser216 (Fig. 4c). Consequently, the mutant proteins failed to bind 14-3-3 protein efficiently (Fig. 4d,e; Supplementary Fig. 8c,d) and remained in the nucleus even during interphase (Fig. 4f; Supplementary Figs 10 and 11). In accordance with these observations, CDC25C mutants enhanced mitotic entry, which was exaggerated by low-dose radiation-induced DNA damage (Fig. 4g,h; Supplementary Fig. 12; Supplementary Methods). These results suggest that mutation of *CDC25C* results in disruption of the DNA checkpoint machinery. Next, we investigated why mutation of *CDC25C* is a frequent genetic event in FPD/AML. It is known that *RUNX1* mutations suppress DNA damage repair and subsequent cell cycle arrest in hematopoietic cells by means of transcriptional suppression of several genes that are involved in DNA repair[12,13]. We confirmed that FPD/AML-associated *RUNX1* mutations have similar effects, as we observed activation of the G2/M checkpoint mechanism in the presence of *RUNX1* mutations (Fig. 4i; Supplementary Fig. 13a,b). We found, however, that introduction of mutations in *CDC25C* resulted in enhanced mitosis entry, despite co-existence of *RUNX1* mutations (Fig. 4i). Therefore, we speculated that compromised DNA damage checkpoint mechanisms caused by mutations in *CDC25C* may contribute to malignant transformation, in concert with increased genomic instability due to *RUNX1* mutations.

Discussion

Whole-exome sequencing, followed by targeted deep sequencing, identified novel aspects of the pathogenesis of malignant transformation in FPD/AML. First, the high frequency of *CDC25C* mutations in FPD/AML underscores their major role in the development of haematological malignancies in FPD/AML patients. To our knowledge, *CDC25C* mutations have not been reported previously and represent a new recurrent mutational target in haematological malignancies, although *CDC25C* mutations have been reported in some solid carcinomas with unknown significance[14,15]. Furthermore, our functional assays support their biological significance, which is characterized by cell cycle progression and premature mitotic entry. Although the 5q31 minimally deleted region, in which CDC25C is located, is frequently detected in MDS, it seems to be associated with other oncogenic mechanisms since our functional assays suggested that *CDC25C* mutations in FPD/AML were gain-of-function type mutations that facilitate the mitotic entry by aberrant accumulation in the nucleus. Impaired DNA repair function mediated by germline *RUNX1* mutation may play a role in the generation of *CDC25C* mutations.

Evaluation of the allelic burden of mutated genes demonstrated that *CDC25* mutations are found with high VAFs in FPD/AML-derived leukaemia and with low VAFs in cases of thrombocytopenia. Our hierarchical model and clonal selection highlighted that mutation of *CDC25C* defines an initial event during malignant transformation and predates subclonal mutations in *GATA2* and other genes. On the basis of the observation that four of the seven FPD/AML patients with *CDC25C* mutations have developed leukaemia and that *CDC25C* mutations were actually detected in the leukaemic subclones, we speculated that a FPD/AML patient with a *CDC25C* mutation, but without clinically evident leukaemia, is at high risk for the onset of leukaemic progression. Examination of the allelic burden of *CDC25C* mutation may thus serve to evaluate the risk of leukaemic progression in patients with FPD/AML.

Among the mutations found in FPD/AML, mutations in *GATA2* were identified in 3 of 13 individuals (subjects 18, 20 and 22). *GATA2* mutations were frequently identified in FPD/AML-derived leukaemia (2/7) and in a patient with thrombocytopenia who had a small subclone bearing a *CDC25C* mutation (1/6). Although reports on the clinical relevance of *GATA2* mutations in myeloid malignancy are limited, several lines of evidence in this respect have recently been reported. *GATA2* mutations are frequently found in a subgroup of patients with cytogenetically normal AML with biallelic *CEBPA* gene mutations[16], which account for ~4% of AML. Germline *GATA2* mutations are also observed in disorders linked to an increased propensity for the development of MDS and AML, including Emberger syndrome, MonoMAC syndrome and dendritic cells, monocytes, B and natural killer cells deficiency[17–20]. The alterations in *GATA2* (leading to p.Leu321His and p.Leu359Val), which were found in FPD/AML patients in this study, are located in the part of the gene encoding the N-terminal and C-terminal zinc-finger domains, respectively (Fig. 3d). Mutations affecting the identical amino acids have been reported in AML patients bearing *CEBPA* mutations and chronic myeloid leukaemia patients in blast crisis[16,21]. Thus, *GATA2* mutation may contribute to AML progression in collaboration with *RUNX1* and/or *CDC25C* mutations. Furthermore, although

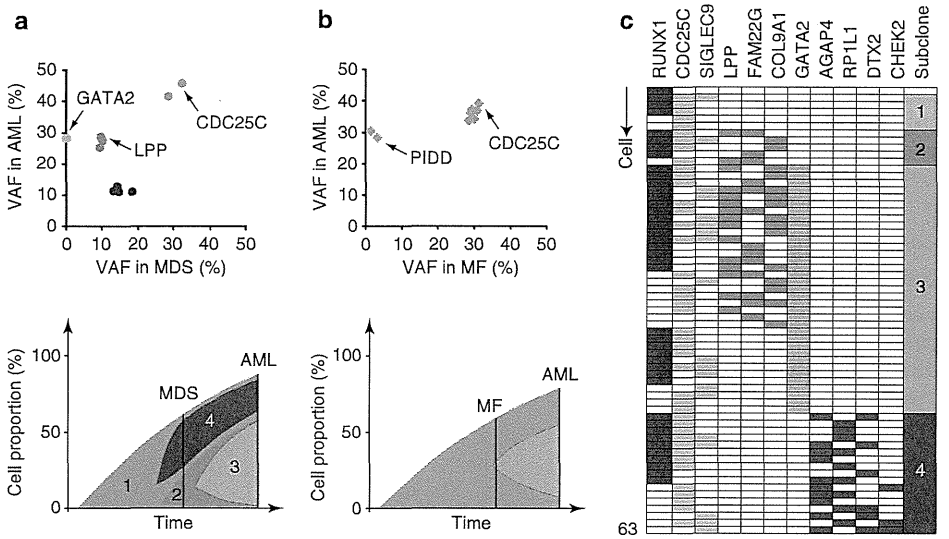

Figure 2 | Clonal evolution of FPD/AML-related myeloid disorders. (**a**,**b**) Observed variant allele fraction (VAF) of validated mutations are listed in Table 2, in both pre-leukaemic and leukaemic phases, are shown in diagonal plots (top) for subject 20 (**a**) and subject 21 (**b**). Predicted chronological behaviours in different leukemia subclones are depicted below each diagonal plot. Distinct mutation clusters are displayed by colour. The vertical axis represents cell proportion of each clone calculated by VAF × 2 (%) (because all the mutations were heterozygous), regarding the whole bone marrow as 100%. (**c**) Mutation status of each bone marrow cell from subject 20 during the acute myeloid leukemia (AML) phase. The vertical axis represents each cell ($n = 63$) and the horizontal axis displays each gene mutation. Coloured columns show that the corresponding cell harbours gene mutation(s) as defined in Online Methods. Subclone numbers shown in the right row correspond to the numbers in the lower figure of **a**.

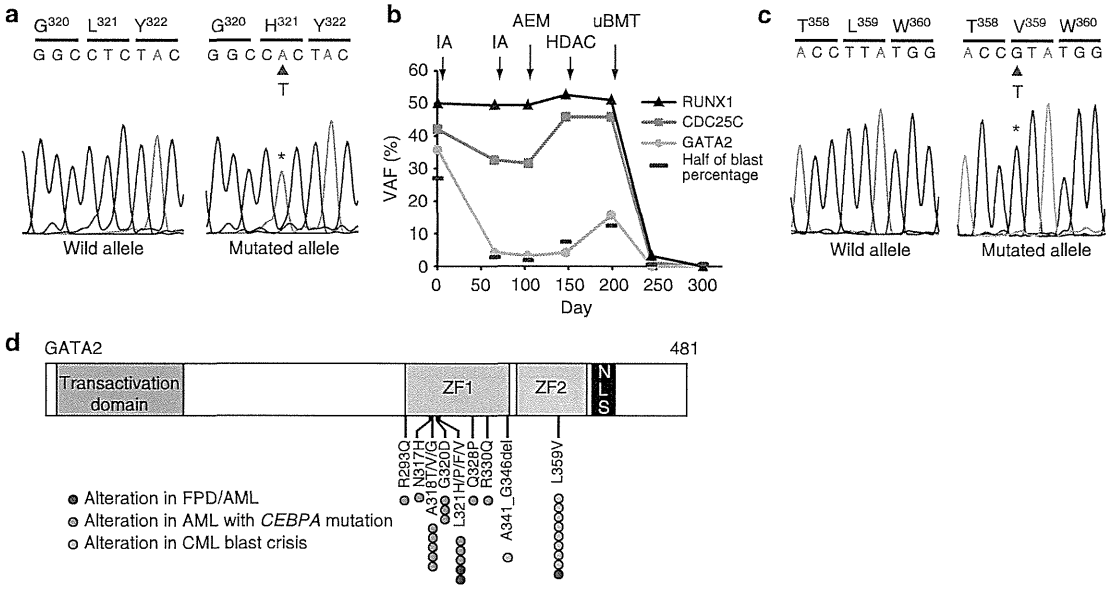

Figure 3 | *GATA2* mutations in FPD/AML. The result of Sanger sequencing for *GATA2* p.Leu321His mutation in subject 22 (**a**) and Leu359Val mutation in subject 18 (**c**) validated with subcloning strategy by methods shown in Supplementary Methods. (**b**) Variant allele fractions (VAFs) of *RUNX1*, *CDC25C* and *GATA2* mutation in subject 22 are demonstrated with the time course of treatment. Half the value of the blast cell percentage, which corresponds to the allele frequency of a heterozygous mutation, is also shown by a red bar. IA, idarubicine + Ara-C; AEM, Ara-C + etoposide + mitoxantrone; HDAC, high-dose Ara-C; uBMT, unrelated bone marrow transplantation. (**d**) Schematic representation of *GATA2* mutations. *GATA2* mutations that were identified in FPD/AML are displayed together with mutations found in AML with *CEBPA* mutation[16] as well as in CML patients in blast crisis[21]. ZF, zinc-finger domain; NLS, a putative nuclear localization sequence domain.

another report identified somatic *CBL* mutation with acquired 11q uniparental disomy as a second hit as being responsible for leukaemic transformation in FPD/AML[22], *CBL* mutations were not detected in our series of FPD/AML samples.

Although the precise pathogenetic roles of *CDC25C* mutations remain unclear, we presume that mutant CDC25C alleles confer a proliferative advantage under certain circumstances in which DNA repair machinery is compromised, such as that mediated by